NASA Technical Memorandum 110144

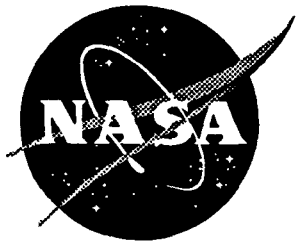

Analysis of Corner Cracks at Hole by a 3-D Weight Function Method with Stresses from Finite Element Method

W. Zhao
University of South Carolina, Columbia, South Carolina

J. C. Newman, Jr.
Langley Research Center, Hampton, Virginia

M. A. Sutton
University of South Carolina, Columbia, South Carolina

X. R. Wu
Institute of Aeronautical Materials, Beijing, Peoples Republic of China

K. N. Shivakumar
North Carolina A&T State University, Greensboro, North Carolina

July 1995

National Aeronautics and
Space Administration
Langley Research Center
Hampton, Virginia 23681-0001

Analysis of Corner Cracks at Hole by a 3-D Weight Function Method with Stresses from Finite Element Method

W. Zhao[1], J.C. Newman, Jr.[2], M.A. Sutton[1], X.R. Wu[3] and K.N. Shivakumar[4]

[1] *University of South Carolina, Columbia, SC 29208, U.S.A.*

[2] *NASA Langley Research Center, Hampton, VA 23681, U.S.A.*

[3] *Institute of Aeronautical Materials, Beijing 100095, P.R. China*

[4] *North Carolina A & T State University, Greensboro, NC 27410, U.S.A.*

ABSTRACT Stress intensity factors for quarter-elliptical corner cracks emanating from a circular hole are determined using a 3-D weight function method combined with a 3-D finite element method. The 3-D finite element method is used to analyze uncracked configuration and provide stress distribution in the region where crack is to occur. Using this stress distribution as input, the 3-D weight function method is used to determine stress intensity factors. Three different loading conditions, i.e. remote tension, remote bending and wedge loading, are considered for a wide range in geometrical parameters. The significance in using 3-D uncracked stress distribution and the difference between single and double corner cracks are studied. Typical crack opening displacements are also provided. Comparisons are made with solutions available in the literature.

1. INTRODUCTION

The weight function method in linear elastic fracture mechanics originated from Bueckner's pioneering work [1], but the widespread acceptance of the method is largely attributed to the discussion and extension made by Rice [2]. The attraction of the method is the separation of the geometry property of a cracked configuration from the applied load. The theory [1,2] shows that once the weight function is known for a cracked configuration, stress intensity factors for the cracked configuration under any applied load can be obtained by a quadrature of the product of the weight function and the stress distribution induced by the applied load acting on the same geometrical configuration but without a crack (also designated as uncracked stress

distribution). It is this feature that gives the weight function method an advantage in dealing with various complex loading conditions. Indeed, extensive research and applications have been performed on the weight function method, and accurate weight functions for various 2-D crack problems of practical interest are now available (see, for example, Wu and Carlsson [3]). For 3-D crack problems, however, this is not the case. The general 3-D weight function theory has long been established independently by Rice [2] and Bueckner [4]. On one hand, this general theory is applicable to any 3-D crack problems and has much wider use than determination of stress intensity factors under various loading conditions [5]. On the other hand, the determination of the 3-D weight functions based on this general theory requires considerable effort, because the weight functions can only be determined by various sophisticated numerical methods, such as the boundary element method [6], the 3-D finite element method [7,8], and the 3-D finite element alternating method [9], with the exception of half-plane cracks or a circular crack in an infinite domain, and cracks perturbed from these [10,11].

If our purpose is to determine stress intensity factors for plane cracks with elliptic-arc front under various loading conditions, as is often the case, alternative approaches in developing 3-D weight function methods are available, which involve further assumptions. The most popular approach, as evidenced by a vast literature, is to adopt the "root mean square" concept proposed by Besuner [12], and often uses Newman and Raju's stress intensity factor equations [13,14] as the reference solutions in developing weight functions. Some typical work can be found in [15-19]. This approach, although very useful, only produces averaged stress intensity factors around the ends of the two axes of an elliptic crack, and can not reflect variations of stress intensity factors along the crack front.

A different approach has been developed and applied to several typical cracked configurations by the present authors [20-27]. The accuracy of the method has been established through comparison with exact or well accepted numerical solutions, such as those in [13,28-33]. In addition to its accuracy and efficiency, the 3-D weight function method [20] has two other advantages: (i) it gives the distribution of stress intensity factors along the crack front and (ii)

in many cases it does not require any reference solutions for the 3-D cracks in question. This latter advantage allows the method to produce independent solutions [20-23], and to solve problems for which no solutions exist, as shown in [24-26]. However, the weight functions in these previous work are limited to relative crack sizes, $a/t \leq 0.6$.

The other element needed in weight function methods is the uncracked stress distribution at the crack location induced by the applied load. This information is often readily obtainable using 2-D theory of elasticity. However, special attention is needed for cracks emanating from stress concentrations, such as a hole or a notch. In such cases, stresses obtained from 2-D theory of elasticity may not represent satisfactorily the true stress distribution, if the hole or notch radius is small compared with the plate thickness. This effect is particularly significant for small cracks, and hence could have significant influence on the predicted fatigue crack life. Although this issue is important, it has not been properly addressed in the literature. There are 3-D solutions for stress concentration factors [34,35] which are helpful in analyzing fatigue crack initiations, but weight function methods require knowledge of the complete stress distribution in the crack region.

The problems to be considered in this work involve both single or double corner cracks emanating from a circular hole in a wide, finite thickness plate. This crack configuration represents one of the most common sources of failures in aircraft structures, and has received considerable attention in the literature. Using a 3-D finite element method, Hechmer and Bloom [36] analyzed double corner cracks under remote tension. The most refined 3-D finite element analysis and extensive solutions were provided by Raju and Newman [28] for double corner cracks under remote tension, remote bending and wedge loading in the hole. Grandt and Kullgren [37] obtained a generalized solution for a single corner crack under crack face pressure loading by a finite element alternating method. Using an improved finite element alternating method, Nishioka and Atluri [38] considered double corner cracks. The weight function method has also been used to provide additional solutions for remote tension [23] by using 2-D uncracked stress distribution.

The present work uses a combined approach of the 3-D weight function method and the 3-D finite element method in analyzing the corner cracked hole. The 3-D finite element method is used to analyze the uncracked hole under remote tension, remote bending, and wedge loading in the hole. The uncracked normal stress distribution under these three load conditions are determined for hole-radius-to-plate-thickness ratios of r/t=0.1, 0.25, 0.5, 1, 1.5 and 2.5. To facilitate the weight function application, these uncracked stress distributions are then fitted by polynomials. The 3-D weight function method [20] is first extended to cover a relative crack depth $a/t \leq 0.9$, and to consider stress variations in the plate thickness direction. Then, with the uncracked stress distribution provided by the 3-D finite element method, the 3-D weight function method is used to determine stress intensity factors for corner cracked holes under remote tension, remote bending and wedge loading in the hole. The geometrical parameters considered in this work are: r/t=0.1, 0.25, 0.5, 1, 1.5 and 2.5; a/c=0.2, 0.4, 1 and 2; a/t=0.01, 0.1, 0.2, 0.3, 0.4, 0.5, 0.6, 0.7, 0.8 and 0.9, within the limit of crack-length-to-hole-radius ratio of 2. The importance for using 3-D stress solutions in determining stress intensity factors by weight function methods is investigated. Also studied is the difference in stress intensity factors between single and double corner cracks. Some typical crack face displacements are provided as well.

NOMENCLATURE

a, c = semi-axes of a quarter-elliptical crack

a_x, c_y = crack length for a- and c-slices

b = half plate width

COD = dimensionless crack face displacement

E = elastic modulus

E_a, E_c = elastic modulus for a- and c-slices

E_s = elastic modulus for spring slices

F = dimensionless stress intensity factor

h = half plate height

k_a, k_c = stretching stiffness of restraining springs

K = stress intensity factor

K_a, K_c = stress intensity factors for a- and c-slices

P(x,y) = coupling force on the crack surface

Q = shape factor of an ellipse

r = hole radius

r_a, r_c = dimensionless restraining area for a- and c-slices

R_a, R_c = restraining area for a- and c-slices

t = plate thickness

T = transition factor

V = crack face displacement

V_a, V_c = crack face displacement for a- and c-slices

W_a, W_c = weight functions for a- and c-slices

x, y, z = Cartesian coordinates

η = an interpolation function at the free surface

ν = Poisson ratio

σ = remote tensile stress

$\sigma(x,y)$ = stress on the crack surface

σ_0 = a reference stress

φ = parametric angle of an elliptical crack

Φ = the complete elliptic integral of the second kind

2. THE 3-D WEIGHT FUNCTION METHOD

Instead of starting from the general 3-D weight function theory [2,4], another form for the 3-D weight function method [20] was developed using the slice synthesis model [39-41], the general weight function expressions for 2-D crack problems [42,43], and the exact solutions for a pressurized embedded elliptical crack in an infinite body [44]. The basic idea of this approach

is to decompose a 3-D cracked body into two types of orthogonal slices of infinitesimal thickness. Each slice is assumed to be in a generalized plane stress state while containing a through-thickness crack. The properties of the 3-D cracked body are built into the slices by considering two effects: (i) the mechanical coupling between adjacent slices and (ii) the restraining effect of the uncracked area on the cracked slices. The 3-D property of a plane crack with elliptic-arc front is further assumed to be divisible into two parts: (1) the fundamental part that is common to all such cracks regardless of (a) their configuration (corner crack, surface crack or embedded crack), (b) the relative size of the crack with respect to the width or thickness) or (c) loading condition and (2) the particular part that depends on the given configurations and loading conditions. The fundamental part of the solutions is obtained by using the known exact stress and crack face displacement solutions for a pressurized embedded elliptical crack in an infinite body [44]. This is one of two reasons why, in many cases, the present method does not require any reference solutions for the 3-D crack in question. Let us elaborate on the method by considering the corner cracked hole in question. For brevity, we will focus on double corner cracks in describing the method.

2.1 Modeling and the Weight Functions

Figure 1 shows the configuration to be considered. Although remote tension is shown, any other mode I loading can be analyzed. This cracked body is decomposed, as per Fig.2, into two types of orthogonal slices of infinitesimal thickness. Each slice is assumed to be in a generalized plane stress state. The symbols R_a and R_c in Fig.2, defined as the restraining areas, represent the uncracked area outside the sliced region. The slices parallel to the a-axis of the crack are designated as a-slices and those parallel to the c-axis as c-slices. The subscripts a or c are used to denote quantities corresponding to a- or c-slices. Note that a-slices correspond to edge-cracked configurations whereas c-slices correspond to center crack configurations as shown in Figs.3(a) and 3(b), respectively. Referring to Figs.3, another distinction needs to be made: basic slices and spring slices. The a-slice in Fig.3(a) is designated as a basic slice, because the thin slice is subjected to the same applied load σ, and has the same elastic modulus, E, as the

3-D cracked body. The c-slice in Fig.3(b) is called a spring slice, because it is subjected to no externally applied load, and has a different elastic modulus, E_s, which will be described latter. The loading of the spring slices in Fig.3(b) is such that the superposition of the two kinds of slices satisfies the loading condition of the original 3-D crack problem. For now, note that in Figs.3 the springs are placed on the slices' boundaries towards which the crack extends and the distributed forces, P(x,y), are applied to the crack faces. These two elements simulate, respectively, the restraining effect due to the uncracked area R_i, and the mechanical coupling between the adjacent basic slices due to the internal stress present on the free-body diagram of an a-slice. P(x,y) is the z-component of the uncracked stress induced by all the internal coupling stresses acting on an a-slice's surface. It is noted that representing the internal coupling stress by P(x,y) is sufficient, involving no assumption, and is justified by the superposition principle. The other components of the uncracked stress, which are not normal to the crack surface, play no role in the model for mode I crack problems and can be discarded. Thus, all the 3-D properties necessary for considering mode I crack problems have, in principle, been incorporated into the slice models and hence their effects can be represented.

Before determining P(x,y) (the load aspect) we need to consider the weight function (the geometry aspect). The slices shown in Figs.3 have elastic boundary constraints exerted by constraining springs with stiffness k_i, (i=a,c). To represent the constraining effect of the uncracked area outside the sliced region, the stiffness k_i is a function of restraining area R_i, (i=a,c). Using a properly non-dimensionalized form for R_i, we have

$$r_a = \frac{R_a}{c^2} = 2\frac{a}{c}\left(\frac{b}{c} - \frac{r}{t}\frac{t}{a}\frac{a}{c} - 1\right)\frac{t}{a} \tag{1a}$$

$$r_c = \frac{R_c}{a^2} = 2\frac{c}{a}\left(\frac{b}{c} - \frac{r}{t}\frac{t}{a}\frac{a}{c}\right)\left(\frac{t}{a} - 1\right) \tag{1b}$$

in which r_i, (i=a,c), varies from 0 to ∞. In general, k_i, as a function of r_i, can not be determined without embarking upon 3-D analysis. However, the following judgement can be made: k_i is a monotonic function of r_i. That is, $k_i \to 0$ as $r_i \to 0$ (which is the case shown in Fig.4) and $k_i \to \infty$ as $r_i \to \infty$ (which is the case shown in Fig.5). Thus, these two limiting conditions serve as the lower and the upper bounds for the slices in Figs.3. Based on these bounding conditions we can construct the weight functions for the slices shown in Fig.3 as following,

$$W_i = W_{2D,i}^{\ fixed} + T_i(r_i)(W_{2D,i}^{\ free} - W_{2D,i}^{\ fixed}) \tag{2}$$

where W_i (i=a,c) is the weight function for the slices in Fig.3. $W_{2D,i}^{\ fixed}$ and $W_{2D,i}^{\ free}$ are the weight functions for the 2-D cracks with fixed boundary condition (Fig.5) and with free boundary condition (Fig.4), respectively. $T_i(r_i)$, designated as the transition factor, is an unknown function of restraining area, r_i, which satisfies $T_i(\infty)=0$, and $T_i(0)=1$. Although eq.(2) reduces the determination of the weight functions for the slices in Fig.3 to the determination of the transition factor $T_i(r_i)$, as was done for an embedded elliptical crack [20], it will not change the fact that in general it can not be determined without 3-D analysis. However, eq.(2) does tell us that if $T_i(r_i)=0$, the first term $W_{2D,i}^{\ fixed}$ alone can be used as W_i. Mathematically, this corresponds to $r_i=\infty$, situations that infinite width and/or thickness dimensions will result in. Physically, the situations where $W_{2D,i}^{\ fixed}$ can be used as W_i are not limited to the cases of $r_i=\infty$. $W_{2D,i}^{\ fixed}$ applies to a wide range of cases in which the presence of a crack will not cause localized deformation on the boundary surfaces where the constraining springs of the slices act. Previous applications [20,22,23,27] based on $W_{2D,i}^{\ fixed}$ have shown very good agreement with finite element solutions for $a/t \leq 0.5$ and finite but large r_i. Other cases where $W_{2D,i}^{\ fixed}$ is used as W_i are situations where the problems have symmetric surfaces that can be taken as one of the slice's boundaries; the constraining springs are replaced by rigid springs. Various problems of this type were solved in [24-26].

We consider the case of infinite width, that is (c+r)/b=0. The particular weight functions W_i for our case are

$$W_a = W_{de}(a_x, y) \tag{3a}$$

$$W_c = W_{h2}(c_y, x) \tag{3b}$$

where W_{de} is the weight function for double edge cracks and W_{h2} is the weight function for two symmetric cracks emanating from a hole in an infinite plate. W_{de} used in previous work was limited to $a/t \leq 0.6$. It is extended to $a/t \leq 0.9$ in this work by using Wu and Carlsson's recent work [3], and is given in Appendix A of this paper.

2.2 **Solution Procedures**

As mentioned earlier, the solution to a 3-D crack problem is divided into two parts: the fundamental part, and the particular part. These will be described in the following section.

2.2.1 **Fundamental Part**

This part of the solutions provide the fundamental relations between (a) the elastic moduli of basic slices and spring slices, (b) the stress intensity factors for a 3-D cracked body and the slices and (c) crack face displacements for a 3-D cracked body and the slices. The first relation determines the elastic modulus of the spring slices. The second and the third relations allow the determination of stress intensity factors and crack face displacements for a 3-D cracked body by using the stress intensity factors and crack face displacements for the slices. These relations have been obtained [20] by calibrating the method against the exact solutions for stress intensity factors and crack face displacements of a pressurized embedded elliptical crack in an infinite body [44]. These relations [20] are given below with brief discussions.

2.2.1.i Elastic Modulus of Spring Slices

The spring slices are devised to represent the mechanical coupling between adjacent basic slices, which is modeled by springs. While the spring force is a function of applied loads and configuration parameters, the stiffness of the spring can be reasonably assumed to be a function of material and the crack aspect ratio only. The result is

$$\frac{E_s}{E} = \left(\frac{\Phi}{1-\nu^2} - 1\right)\frac{c}{a} \qquad a/c \le 1 \tag{4a}$$

$$\frac{E_s}{E} = \frac{\Phi}{1-\nu^2} - \frac{c}{a} \qquad a/c > 1 \tag{4b}$$

where ν is the Poisson's ratio and Φ is the complete elliptic integral of the second kind.

2.2.1.ii Stress Intensity Factors and Crack Face Displacements

Referring to Fig.6 for definition of crack parameters, the following equation gives the relation between stress intensity factors $K(\varphi)$ for a 3-D crack at location φ on the crack front, and the stress intensity factors K_i for the two orthogonal slices intersecting at a common point (x,y),

$$K(\varphi) = \frac{(-1)^n}{1-\nu^2}\left\{K_a^4(x,a_x) + \left[\frac{E}{E_s}K_c(y,c_y)\right]^4\right\}^{\frac{1}{4}} \tag{5}$$

where $n=1$ for $K_i \le 0$ and $n=2$ for $K_i > 0$. The crack face displacement V(x,y) for a 3-D crack is equal to the crack face displacements for the slices. Thus,

$$V(x,y) = V_a(a_x,y) = V_c(c_y,x) \tag{6}$$

The validity of equations (5) and (6) has been proved analytically for a pressurized embedded elliptical crack in an infinite body [20], and numerically for various cracks of elliptic-arc front

in finite bodies under a variety of loading conditions, see, for example, [20,22,23], indicating that the assumptions made in the method are valid.

2.2.2 **Particular Part**

This part of the solution process for a 3-D crack problem deals with the particular geometry and loading conditions for the problem in question. The stress intensity factors and crack face displacements for both types of orthogonal slices are determined, with the aid of the fundamental solution in the first part of this section, by using 2-D weight function theory [1-3]. Then the stress intensity factors and the crack face displacements for the 3-D crack are obtained by using the fundamental relations given above. Since we consider an infinite width plate, our slices are reduced to those in Fig.5. Their weight functions are given in eq. (3).

Using the 2-D weight function theory [1-3], the stress intensity factors for the slices are

$$K_a(x,a_x) = \int_0^{a_x} [\sigma(x,y) - P(x,y)]\, W_{de}(a_x,y)dy \tag{7a}$$

$$K_c(y,c_y) = \int_0^{c_y} P(x,y) W_{h2}(c_y,x)dx \tag{7b}$$

The crack face displacements for the slices are

$$V_a(a_x,x,y) = \frac{1}{E_a}\int_y^{a_x} K_a(x,\xi) W_{de}(\xi,y)d\xi \tag{8a}$$

$$V_c(c_y,x,y) = \frac{1}{E_c}\int_x^{c_y} K_c(y,\xi) W_{h2}(\xi,x)d\xi \tag{8b}$$

in which $E_a=E$, $E_c=E_s$, which is given by eq. (4). The only unknown in these equations is the spring force P(x,y), which can be determined by the compatibility requirement on the crack face displacements. That is,

$$V_a(a_x,x,y)=V_c(c_y,x,y) \tag{9}$$

The resulting integral equation for P(x,y) reads as,

$$\int_y^{a_x}\left\{\int_0^{\xi}\sigma(x,y)W_{de}(\xi,y)dy\right\}W_{de}(\xi,y)d\xi = \int_y^{a_x}\left\{\int_0^{\xi}P(x,y)W_{de}(\xi,y)dy\right\}W_{de}(\xi,y)d\xi+\frac{E_a}{E_c}\int_x^{c_y}\left\{\int_0^{\eta}P(x,y)W_{h2}(\eta,x)dx\right\}W_{h2}(\eta,x)d\eta \tag{10}$$

To solve this equation, the unknown spring force P(x,y) is expressed as a polynomial function of x and y:

$$\begin{aligned}P(x,y)/\sigma_0=&\lambda_1+\lambda_2(x/c)^{1/3}+\lambda_3(y/a)^{1/3}+\lambda_4(x/c)+\lambda_5(y/a)+\lambda_6(x/c)(y/a)+\lambda_7(x/c)^2+\lambda_8(y/a)^2\\&+\lambda_9(x/c)^{1/3}(y/a)^{1/3}+\lambda_{10}(x/c)^2(y/a)^2+\lambda_{11}(x/c)^3+\lambda_{12}(y/a)^3+\lambda_{13}(x/c)^4+\lambda_{14}(y/a)^4\\&+\lambda_{15}(x/c)^{1/3}(y/a)+\lambda_{17}(x/c)(y/a)^{1/3}+\lambda_{17}(x/c)(y/a)^2+\lambda_{18}(x/c)^2(y/a)\end{aligned} \tag{11}$$

where σ_0 is a reference stress. The 1/3 terms are included because of their beneficial effect observed when each term was examined individually. Let eq. (11) be written in the abbreviated form

$$P(x,y)=\sigma_0\sum_{j=1}^{l_0}\lambda_j p_j(x,y) \tag{12}$$

where $l_0=18$. Substituting eq. (12) into (10), the result can be expressed in the form

$$Y(x,y)=\sum_{j=1}^{k_0}\lambda_j X_j(x,y) \tag{13}$$

where

$$Y(x,y)=\int_y^{a_x}\left\{\int_0^{\xi}\sigma(x,y)W_{de}(\xi,y)dy\right\}W_{de}(\xi,y)d\xi \tag{14}$$

$$X_j(x,y)=\int_y^{a_x}\left\{\int_0^{\xi}p_j(x,y)W_{de}(\xi,y)dy\right\}W_{de}(\xi,y)d\xi+\frac{E_a}{E_c}\int_x^{c_y}\left\{\int_0^{\eta}p_j(x,y)W_{h2}(\eta,x)dx\right\}W_{h2}(\eta,x)d\eta \tag{15}$$

These integrals represent the crack face displacements. To avoid double numerical integration, the inner integrals in the above expressions, which represent the stress intensity factors, are evaluated analytically. The remaining integrals are determined at 44 different locations as shown in Fig.7. These points are chosen based on the considerations of: (1) symmetry about the x- and y-axes, and (2) sufficient distribution over the entire crack surface. The 44 data points are sufficient such that a further increase in the data points will not change the results. Then the resulting redundant system of simultaneous equations for λ_j is solved by a multiple linear regression scheme. Once λ_j is known, P(x,y), the value for K_i and V_i are determined. Then, $K(\varphi)$ and V(x,y) are obtained by using the fundamental relations given in the first part of this section. However, one modification should be included in eq.(5), which is for a crack whose entire front is in a local plane strain field. For part-elliptical cracks, the crack front intersects the free surface, and the local plane strain field no longer exists at this point. This is accounted for in Appendix B.

2.3 **3-D Uncracked Stress Distribution**

The uncracked stress distribution, $\sigma(x,y)$, used in the weight function method was obtained by the 3-D finite element analysis [35]. To facilitate its application, the uncracked stress distribution was then fitted into the following equation:

$$\sigma(x,y)/\sigma_0 = \sum_{i=1}^{I}\sum_{j=1}^{J} C_{ij}\left(\frac{x}{r}+1\right)^{2-2i}\left(\frac{y}{t}-\frac{1}{2}\right)^{q} \tag{16}$$

where q=2j-2 for remote tension and wedge loading, and q=2j-1 for remote bending. The σ_0 is a reference stress and $\sigma_0=\sigma_t=\sigma$ for remote tension; $\sigma_0=\sigma_w=P/(2rt)$ for wedge loading and $\sigma_0=\sigma_b$ (remote outer fiber bending stress) for remote bending. The applied load in the hole is P.

3. RESULTS AND DISCUSSIONS

Using the uncracked stress distributions given by the 3-D finite element method, comprehensive solutions of stress intensity factors for a corner cracked hole under remote tension, remote bending and wedge loading in the hole will be provided in the following section by the 3-D weight function method. The results are compared, whenever possible, with existing solutions. The importance of using 3-D uncracked stress solutions in weight function methods is studied by comparing stress intensity factor solutions obtained from using 2-D and 3-D uncracked stress distributions. The difference in stress intensity factors between single and double corner cracks is investigated. Some typical results for crack face displacements are also provided.

The stress intensity factors are given in a dimensionless form defined as

$$F(\varphi)=K(\varphi)/(\sigma_o\sqrt{\pi a}/\Phi) \tag{17}$$

Some typical crack mouth (x=y=0) displacements are given in the following dimensionless form:

$$COD = \frac{V(0,0)E}{c\sigma_0} \tag{18}$$

3.1 Stress Intensity Factors for Double Corner Cracks

3.1.1 Remote Bending

The weight function results for double corner cracks under remote bending are listed in Tables 1-6 for r/t=0.1, 0.25, 0.5, 1, 1.5 and 2.5, respectively. Comparisons with finite element solutions [28] are shown in Figs.8 through 10 for a/c=0.2, 2 and 1, respectively. Also shown are the results from Newman and Raju's empirical equations [14]. Before discussing the comparison, we note that the finite element solution [29] was obtained for $(c+r)/b \leq 0.2$, while the weight function solution is obtained by using weight functions for (c+r)/b=0, and stress distributions for r/b=0.2. This difference in the models has minimal effect as long as the restraining areas in the finite element model were large enough to resist localized deformation on the back surface. For the cases of smaller restraining areas, the weight function solutions for infinite width cases will serve as a lower bound of solutions for the cases of finite width. Inspection of Figs.8 through 10 shows that the agreement between weight function and finite element solutions is generally very good, except for the region near the hole surface ($\varphi=90°$) for a/t=0.2, where the precipitous drop-off of the finite element solutions has been shown to be mainly due to some "ill-shaped" elements near the hole surface [31]. Furthermore, the equation [14] generally gives a good estimation in this region, because finite element data in this region were not used in developing the equations [13,14].

3.1.2 Remote Tension

Tables 7-12 list the weight function results for double corner cracks under remote tension with r/t=0.1, 0.25, 0.5, 1, 1.5 and 2.5, respectively. Comparisons with other available solutions are shown in Figs.11 through 13 for a/c=0.2, 2.0 and 1.0, respectively. The general trend can

be divided into three categories by a/c and a/t ratios: (i) a/c=0.2 and 2.0 with a/t≤0.5, (ii) a/c=0.2 and 2.0 with a/t=0.8 and (iii) a/c=1.0.

For category (i) (Figs.11(a,b) and 12(a,b)), the weight function solutions agree very well with various numerical solutions, with excellent agreement observed for a/c=0.2. The weight function solutions and the finite element solutions [28] coincide with each other, except for the region near the hole surface, where the finite element model contained "ill-shaped" elements [31]. It is noted that, for a/c=0.2, detailed convergence studies were performed in the finite element analysis [28]. For a/c=2, good agreement between the weight function method and the finite element alternating method [38] is observed along the entire crack front.

For category (ii), the weight function results and the finite element/finite element alternating results have good agreement around $\varphi=0°$ and for a/t≤0.5, but they differ significantly in a large region towards $\varphi=90°$ (see a/t=0.8 in Figs.12(a,b)), with the weight function solution being higher than the numerical solutions.

For category (iii) (Figs.13(a,b)), the results do not agree, except for a/t=0.2 with r/t=0.5 (Fig.13(a)), where the weight function and the finite element solutions [36] agree within 6%. The weight function results are either equal to or consistently lower than the finite element results [28] for $\varphi\leq45°$, and consistently higher than the finite element results [28] towards $\varphi=90°$.

As shown in Figs.12 and 13, the weight function solutions are higher than the finite element solutions for some cases. However, since the weight functions used are for the cases of maximum constraint, it is expected that the weight function solutions would be either correct or a lower bound for the "true" solutions for the cases of finite restraining areas. Thus, it appears that additional finite element analysis with detailed convergence studies are needed to determine the source of the discrepancies shown in Figs.12 and 13. To further indicate the accuracy of the weight function solution, Figures 14(a,b) show the limiting cases as a/c→0 and ∞. The plane strain condition is assumed at $\varphi=0°$ for a/c≥20 in Fig.14(a) and at $\varphi=90°$ for a/c≤0.05 in Fig.14(b) (see Appendix B for details). In Fig.14(b), a large r/t is used to keep c/r

within the weight function's limit of c/r=2. As observed, the weight function solutions produced the correct limits for 2-D cracks.

3.1.3 **Wedge Loading in the Hole**

The weight function results for double corner cracks under wedge loading in the hole are listed in Tables 13-18 for r/t=0.1, 0.25, 0.5, 1, 1.5 and 2.5, respectively. The 3-D finite element solution of the uncracked stress distribution is for a cosine wedge loading distribution, while the finite element stress intensity factor solutions reported in [28] were for cosine squared distributions. Before comparing the weight function solutions for the cosine distribution with the finite element solutions for the cosine squared distribution, it would be helpful to understand the difference between the two load distributions. Figure 15 shows such a comparison. The 2-D solutions are taken from [38,45]. As shown in Fig.15, the cosine distribution is higher than the cosine squared distribution by 8% at the hole surface (x/r=0), which is the maximum difference (This would make the weight function solution a little higher near φ=90°). The two solutions cross each other at about x/r=0.05 and the two distributions converge as x/r increases; the difference at x/r=1 is about 1%. Figures 17 through 18 show a comparison of the weight function solutions with other available solutions (c/r ratios are given in these Figures to show the crack range in the x-direction). The trend here is the same as that for remote tension, and can be similarly discussed in terms of the same three categories as above. It is noted, however, that improved agreement is observed for category (ii) (a/c=0.2 and 2.0 with a/t=0.8, see Figs.17(a,b)) and category (iii) (see Fig.18(a)).

3.2 <u>Significance in Using 3-D Uncracked Stress Solutions</u>

In the literature, applications of weight function methods to cracks emanating from stress concentrations have invariably used uncracked stress distributions from 2-D analysis. As indicated by 3-D analysis of stress concentration factors [34,35], the 2-D solutions may not represent the true solutions satisfactorily. By using both 2-D [46] and 3-D uncracked stress solutions, Figures 19(a,b) and 20(a,b) compare the weight function solutions obtained for remote tension. Two r/t ratios, 0.5 and 1; and two a/c ratios, 0.2 and 2, are considered. As can be

seen, the difference in stress intensity factors from 2-D and 3-D stress solutions depends on r/t. Since different crack shapes and sizes cover areas having different stresses, it also depends on a/c and a/t, and varies along the crack front. The general trend is: the smaller r/t and a/t, the larger the difference. For the same r/t and a/t ratios, the difference is more pronounced and is retained longer for a/c=2, primarily because the crack front is closer to the hole surface. It is clearly seen that the 2-D stress solution can overestimate the K-factors significantly for small corner cracks. This is of practical importance since most of fatigue life is spent when the crack is small. As the crack gets larger, the crack front gets farther from the corner region formed by the hole surface and the plate surface where the 2-D and 3-D stress solutions differ most. Hence, the difference decreases. However, for small r/t ratios with small a/t ratios, use of the 3-D uncracked stress solutions is necessary.

3.3 Difference between Single and Double Cracks

A single corner crack can be considered by using appropriate weight functions for c-slices. The solutions for a single crack are compared with those for double cracks in Figs.21 and 22 for remote tension and remote bending, respectively. Because of the large a/t and small r/t ratios considered, the differences observed in Figs.21 and 22 are among the largest that corner cracks could have for these load cases. For remote tension, Figure 21(b) compares the ratio K_d/K_s, where K_d is for double cracks and K_s for a single crack. As in Fig.21(a), the same a/t ratio of 0.8 and L/r ratio of 1.005 are used, where L is the length of a through-thickness crack that has the same area as a corner crack. We note that the ratio of K_d/K_s increases with a/c, since the corner crack becomes closer to a through crack. Also shown in Fig.21(b) are the results from Shah's conversion factor [47], and from through-thickness cracks [3]. In the literature, Shah's conversion factor [47] is invariably used to obtain stress intensity factors for single crack by using solutions for double cracks, or vice versa. In this case, Shah's result has an error in the range of 3-11%; it will overestimate K_d or underestimate K_s, depending upon which one is the known solution. Figure 22 compares the same cracks as in Fig.21(a), but under

remote bending. The differences are small. For very small cracks, single crack and double crack configurations will have the same solution.

3.4 Crack Face Displacements

Crack face displacement is a useful parameter in fatigue and fracture experiments, in fatigue crack modeling and in fracture criterion. The crack face displacement is obtained during the process of obtaining K values by the weight function method. Some typical crack face displacements at the crack mouth location (x=y=0) are shown in Fig.23. A large range of a/c ratios from 1 to 80 is considered, as represented by circles in the Figure. Also shown in Fig.23 are the results for through-thickness cracks by Mall and Newman [48], with plane strain conditions assumed. As can be seen, the crack face displacement for corner cracks approaches that for through-thickness cracks as a/c increases (c/r decreases as a consequence). The two coincide for a/c>7 (c/r<0.046). A slight difference (2%) at a/c=80 (c/r=0.004) is due to inaccuracies in the weight function; crack face displacements at other locations are expected to have better accuracy than at the crack mouth.

4. CONCLUDING REMARKS

Through the above analysis and discussions it is shown that the optimal combination of the 3-D weight function method and the 3-D finite element method provides an accurate and efficient approach to analyze 3-D cracks emanating from stress concentrations. Extensive results of stress intensity factors are obtained for remote tension, remote bending and wedge loading in the hole. The configuration parameters covered are r/t=0.1, 0.25, 0.5, 1, 1.5 and 2.5; a/c=0.2, 0.4, 1 and 2; and a/t=0.01, 0.1, 0.2, 0.3, 0.4, 0.5, 0.6, 0.7, 0.8, and 0.9 within the limit of c/r=2. The significance in using 3-D uncracked stress distribution in 3-D weight function methods is demonstrated. This is particularly important to small corner cracks from relatively small holes. The difference in stress intensity factors between a single corner crack and double corner cracks is studied. Typical crack face displacements are also presented. To account for the change of stress state at the intersection of the crack front with the free surface,

an interpolation function is developed. With the aid of the superposition principle the solutions provided can be used to solve many practical problems.

REFERENCES

[1] H.F. Bueckner,A novel principle for the computation of stress intensity factors. ZAMM 50, 529-546 (1970).

[2] J.R. Rice, Some remarks on elastic crack-tip stress fields. Int. J. Solids Structures 8, 751-758 (1972).

[3] X.R.Wu and J.Carlsson, Weight functions and stress intensity factor solutions. Pergamon press, (1991).

[4] H.F. Bueckner, in Methods of analysis and solution of crack problems, G.C. Sih, Ed., Noordhoff, Leyden, the Netherlands, 239-314 (1973).

[5] J.R. Rice, Weight function theory for three-dimensional elastic crack analysis. ASTM STP 1020, R.P. Wei and R.P. Gangloff, Eds., 29-57 (1989).

[6] G.P. Nikishkov and V.A. Piminov, Computation of weight functions for three-dimensional cracks by the boundary element method. Computational Mechanics 9, 211-220 (1992).

[7] D.M. Parks and E.A. Kamenetzky, Weight functions from virtual crack extension. Int. J. Numerical Methods in Engineering 14, 1793-1706 (1979).

[8] T.L. Sham and Y. Zhou, Computation of three-dimensional weight functions for circular and elliptical cracks. Int. J. Fracture 41, 51-75 (1989).

[9] C.Y. Liao and S.N. Atluri, An alternating technique for evaluating weight functions for 3-D surface flaws in finite solid bodies. Int. J. Numerical Methods in Engng. 32, 1339-1361 (1991).

[10] J.R. Rice, First order variation in elastic fields due to variation in location of a planar crack front. Journal of Applied Mechanics 52, 571-579 (1985).

[11] H.F. Bueckner, Weight functions and fundamental fields for penny-shaped and the half plane crack in three-space. Int. J. Solids and Structures 23, 57-93 (1987).

[12] P.M. Besuner, Residual life estimates for structures with partial thickness cracks. ASTM STP 590, 403-419 (1976).

[13] J.C. Newman Jr.and I.S. Raju, Stress intensity factor equations for cracks in three-dimensional finite bodies. ASTM STP 791,(Edited by J.C. Lewis and G. Sines), I-238 - I-256 (1983).

[14] J.C. Newman Jr.and I.S. Raju, Stress intensity factor equations for cracks in three-dimensional finite bodies subjected to tension and bending loads. in Computational Methods in the Mechanics of Fracture, (Edited by S.N. Atluri), 312-334 (1986).

[15] T.A. Cruse and P.M. Besuner, Residual life prediction for surface cracks in complex structural details. J. Aircraft 12, 369-375 (1975).

[16] C. Mattheck, P. Morawietz and D. Munz, Stress intensity factor at the surface and at the deepest point of a semi-elliptical surface crack in plates under stress gradients. Int. J. Fracture 23, 201-212 (1983).

[17] R. Perez, S.K. Ray and A.F. Grandt, Jr., Application of a weight function method to predict the fatigue life of corner cracked holes loaded in bending. Engng. Fracture Mech. 28, 283-291 (1987).

[18] T. Fett, The crack opening displacement field of semi-elliptical surface cracks in tension for weight functions applications. Int. J. Fracture 36, 55-69 (1988).

[19] V.A. Vainshtok and I.V. Varfolomeyev, Stress intensity factor analysis for part-elliptical cracks in structures. Int. J. Fracture 46, 1-24 (1990).

[20] W. Zhao, X.R. Wu and M.G. Yan, Weight function method for three dimensional crack problems-I & II. Engng. Fracture Mech. Vol.34, No.3, 593-607, 609-624 (1989).

[21] W. Zhao and X.R. Wu, Stress intensity factors for corner cracks at a semi-circular notch under stress gradients. Fatigue and Fracture Engng. Mater. Struc. Vol. 13, 347-360 (1990).

[22] W. Zhao and X.R. Wu, Stress intensity factor evaluation by weight function method for surface crack in edge notch. Theoretical and Applied Frac. Mech. 13, 225-238 (1990).

[23] W. Zhao, X.R. Wu and M.G. Yan, Stress intensity factors for corner cracks at a hole under remote tension. Acta Mechanica Sinica, Vol. 7, 76-81 (1991).

[24] W. Zhao, Analysis of uniformly-spaced coplanar embedded elliptical cracks. Engg. Fracture Mech. 38, 313-319 (1991).

[25] W. Zhao, Analyses of four symmetric corner cracks in elastic plates. Fatigue and Fracture Engg. Mater. Struc. 15, 339-346 (1992).

[26] W. Zhao, Analyses of infinite pairs of surface cracks in elastic plates. Int. J. Fracture, 55, 143-152 (1992).

[27] J.C. Newman, Jr., X.R. Wu, M.H. Swain, W. Zhao, E.P. Phillips, C.F. Ding, Small crack growth behavior in high strength aluminum alloys - A NASA/CAE Cooperative Program, in Proc. 18th Congress of the International Council of the Aeronautical Sciences, Beijing, China, ICAS-92-5.4.3 (1992).

[28] I.S. Raju and J.C. Newman, Jr., Stress intensity factors for two symmetric corner cracks. ASTM STP 677, C.W. Smith, Ed., 411-430 (1979).

[29] J.C. Newman, Jr. and I.S. Raju, Analyses of surface cracks in finite plates under tension and bending loads. NASA TP-1578 (1979).

[30] I.S. Raju and J.C. Newman, Jr., Stress intensity factors for corner cracks in rectangular bars. ASTM STP 969, T.A. Cruse, Ed., 43-55 (1988).

[31] P.W. Tan, I.S. Raju, K.N. Shivakumar and J.C. Newman, Jr., Evaluation of finite element models and stress intensity factors for surface cracks emanating from stress concentrations. ASTM STP 1060, W.G. Reuter, J.H. Underwood and J.C. Newman, Jr., Eds., 34-48 (1990).

[32] K.N. Shivakumar and J.C. Newman, Jr., Stress intensity factors for large aspect ratio surface and corner cracks at a semi-circular notch in a tension specimen. Engng. Fracture Mech. 38, 467-473 (1991).

[33] P.W. Tan, C.A. Bigelow and J.C. Newman, Jr., Three-dimensional finite-element analyses of corner cracks at stress concentrations. in Durability of Metal Aircraft Structures. S.N. Atluri, C.E. Harris, A. Hoggard, N.Miller, and S.G. Sampath, Ed., 187-199 (1992).

[34] E.S. Folias, Some remarks on three-dimensional fracture. ASTM STP 969, T.A. Cruse, Ed., 56-72 (1988).

[35] K.N. Shivakumar and J.C. Newman, Jr., Stress concentrations for straight-shank and countersunk holes in plates subjected to tension, bending, and pin loading. NASA-TP-3193 (1992).

[36] J.L. Hechmer and J.M. Bloom, Determination of stress intensity factors for the corner-cracked hole using the isoparametric singularity element. Int. J Fracture 13, 732-735 (1977).

[37] A.F. Grandt, Jr. and T.E. Kullgren, Stress intensity factors for corner cracked holes under general loading conditions. J. Engng. Materials Technology 103, 171-176 (1981).

[38] T. Nishioka and S.N. Atluri, Integrity analysis of surfaced-flawed aircraft attachment lugs: a new, inexpensive, 3-D alternating method. Paper 82-0742, AIAA/ASME/ASCE/AHS 23rd Structures, Structural Dynamics and Materials Conference, May 10-12, 287-300 (1982).

[39] W.T. Fujimoto, Determination of crack growth and fracture toughness parameters for surface flaws emanating from fastener holes. in Proceedings, AIAA/ASME/SAE 17th Structures, Structural Dynamics, and Material Conference, King of Prussia, Pa., 522-531 (1976).

[40] H.D. Dill and C.R. Saff, Environmental-load interaction effects on crack growth. AFFDL-TR-78-137 (1978).

[41] C.R. Saff and K.B. Sanger, Part-through flaw stress intensity factors developed by a slice synthesis technique, ASTM STP 833, R.J. Sanford, Ed., 24-43 (1984).

[42] X.R. Wu, Approximate weight functions for center and edge cracks in finite bodies. Engng. Fracture Mech. 20, 35-49 (1984).

[43] X.R. Wu, Weight functions and stress intensity factors for radial crack(s) emanating from a circular hole in an infinite sheet. Report 63, TRITA-HEL-0063 ISSN 0281-1502, The Royal Institute of Technology, S-10044 Stockholm, Sweden (1985).

[44] G.R. Irwin, Crack extension force for a part-through crack in a plate. J. Appl. Mech. 29, 651-654 (1962).

[45] D.P. Rooke and J. Tweed, Stress intensity factors for a crack at the edge of a loaded hole. Int. J. Engng. Sci. 18, 109-121 (1980).

[46] S.P. Timoshenko and J.N. Goodier, Theory of Elasticity, McGraw-Hill, 1970.

[47] R.C. Shah, Stress intensity factors for through and part-through cracks originating at a fastener holes. ASTM STP 590, 429-459 (1976).

[48] S. Mall and J.C. Newman, Jr., Crack-surface displacements for two symmetric cracks emanating from a circular hole in an infinite plate. Engng. Fracture Mech. 24, 929-931 (1986).

[49] H.G. deLorenzi, Elastic-plastic analysis of the maximum postulated flaw in the beltline region of a reactor vessel. Rep. No. 82 CRDO 49, General Electric (1982).

Appendix A

The weight function W_{de} in eq. (3a) is taken from Wu and Carlsson [3]. It was developed by making an assumed crack face displacement expression satisfy the following four conditions: (i) K-controlled near-tip crack face displacement, (ii) self-consistent K factor, (iii) vanishing curvature at crack mouth, and (iv) known solution at crack mouth. The resulting weight function has an accuracy better than 2% in K for $a/t \leq 0.85$.

Defining the dimensionless crack length $s=a/t$, the weight function [3] is expressed as follows:

$$W_{de}(s,y)=\frac{1}{\sqrt{2\pi a}}\sum_{i=1}^{5}\beta_i(s)\left(1-\frac{y}{a}\right)^{i-\frac{3}{2}} \tag{A1}$$

where

$$\begin{aligned}
\beta_1 &= 2 \\
\beta_2 &= [4sf'(s)+2f(s)+\frac{3}{2}F_2(s)]/f(s) \\
\beta_3 &= \{sF_2'(s)+\frac{1}{2}[5F_3(s)-F_2(s)]\}/f(s) \\
\beta_4 &= \{sF_3'(s)-\frac{1}{2}[7F_4(s)-3F_3(s)]\}/f(s) \\
\beta_5 &= [sF_4'(s)-\frac{5}{2}F_4(4)]/f(s)
\end{aligned} \tag{A2}$$

where "′" represents differentiation with respect to s, and

$$
\begin{aligned}
F_1 &= 4f(s) \\
F_2 &= \frac{1}{12\sqrt{2}}[315\pi\xi(s) - 105V(s) - 208\sqrt{2}f(s)] \\
F_3 &= \frac{1}{30\sqrt{2}}[-1260\pi\xi(s) + 525V(s) + 616\sqrt{2}f(s)] \\
F_4 &= \sqrt{2}V(s) - [F_1(s) + F_2(s) + F_3(s)]
\end{aligned}
\tag{A3}
$$

$$
\begin{aligned}
\xi(s) &= \frac{1}{s^2}\int_0^s \zeta f^2(\zeta)d\zeta \\
f(s) &= \frac{K}{\sigma\sqrt{\pi a}} \\
V(s) &= \frac{u(s,0)E}{a\sigma}
\end{aligned}
\tag{A4}
$$

in which K and u are reference stress intensity factor and crack mouth displacement, respectively. The reference load case used is a uniform crack face pressure, σ.

Appendix B

The situation at the intersection of the crack front with the free surface differs from that in the interior in two aspects: (i) the order of stress singularity, and (ii) the stress state. The weight function method is unable to address the first issue but, fortunately, the study by the 3-D finite element method has shown that the non-square root singularity dominates only a very thin layer from the free surface, which is less than 3° in terms of crack parametric angle measured from the surface [30]. Furthermore, numerous applications have shown that stress intensity factors obtained without considering the changes in stress singularity produced good correlation to experimental data. Therefore, the change of stress singularity can be neglected from the application point of view.

The modification to eq.(5) is concerned with the change of stress conditions, which occurs in a larger area than that in which the non-square root singularity dominates. The stress

state at the intersection of the crack front with the free surface is in general neither plane strain, nor plane stress, but somewhere in between. The modification to eq.(5) is based on the results from (i) the crack front constraint analysis [49] and (ii) the analysis of embedded elliptical cracks of various a/c ratios [23].

The constraint analysis [49] shows that most of the crack front is nearly in a plane strain state, except for a small region with a parametric angle of about 10° from the surface, where the constraint factor is zero. The analysis of embedded elliptical cracks [24] has shown that for $a/c \geq 20$, the stress intensity factor at the minor axis stays the same as that of a corresponding 2-D center crack. This gives the condition that the stress intensity factor at the minor axis attains the appropriate value of the corresponding 2-D crack when $a/c \geq 20$. In other words, this condition implies that for $a/c \geq 20$, use of an appropriate stress state should make the stress intensity factor at the minor axis equal to that of the corresponding 2-D crack. This appropriate stress state is a plane strain state.

Based on these two considerations, an engineering estimation is adopted, such that an interpolation between plane stress and plane strain is completed as a function of a/c and $\Delta\varphi$, the parametric angle measured from the surface. One way of accomplishing this is to modify eq.(5) as follows:

$$K(\varphi) = \frac{(-1)^n}{1-\eta^2(\nu, a/c, \Delta\varphi)} \left\{ K_a^4(x, a_x) + \left[\frac{E}{E_s} K_c(y, c_y) \right]^4 \right\}^{\frac{1}{4}} \qquad \text{(B1)}$$

where $\eta(\nu, a/c, \Delta\varphi)$ is a bi-quadratic function of a/c and $\Delta\varphi$. The effect of this modification is to realize (i) plane stress conditions for $\Delta\varphi = 0°$ with $a/c = 0$ (at $\varphi = 0°$), or $c/a = 0$ (at $\varphi = 90°$); and (ii) plane strain conditions for $\Delta\varphi \geq 10°$; and for $a/c \geq 20$ (at $\varphi = 0°$), or $c/a \geq 20$ (at $\varphi = 90°$). A bi-quadratic interpolation is used for portions between these extreme points, with slower changes towards $\Delta\varphi = 10°$ and $a/c = 20$. For example, the bi-quadratic function $\eta(\nu, a/c, \Delta\varphi)$ can take the following form (near $\varphi = 0°$):

$$\eta(\nu,a/c,\Delta\varphi)=\frac{\nu^2}{1+\nu}\left\{\frac{1}{\nu}+2\frac{(a/c)}{(a/c)_0}-\frac{(a/c)^2}{(a/c)_0^2}+2\frac{(\Delta\varphi)}{(\Delta\varphi)_0}-\frac{(\Delta\varphi)^2}{(\Delta\varphi)_0^2}-\frac{(a/c)(\Delta\varphi)}{(a/c)_0(\Delta\varphi)_0}\right\} \qquad \text{(B2)}$$

where $(a/c)_0=20$ with $0\leq a/c\leq 20$, and $(\Delta\varphi)_0=10°$ with $0°\leq\Delta\varphi\leq 10°$. A schematic representation of η is given in Fig.B1. The corresponding function for the case near $\varphi=90°$ can be obtained by replacing a/c with c/a in eq. (B2). Finally, it should be pointed out that the maximum difference between eq. (5) and eq. (B1) is only 4% for $\nu=0.3$.

Table 1 Dimensionless stress intensity factors for double corner cracks at a hole under remote bending, r/t=0.1

a/c	a/t	$\varphi°$ 0.1	11.3	22.5	33.8	45.0	56.3	67.5	82.5	89.9
0.2	0.01	0.820	0.826	1.015	1.202	1.393	1.606	1.850	2.285	2.561
0.4	0.01	1.403	1.266	1.383	1.546	1.728	1.939	2.164	2.506	2.684
1.0	0.01	2.645	2.350	2.310	2.313	2.336	2.415	2.513	2.708	2.878
	0.1	1.569	1.380	1.327	1.322	1.356	1.422	1.539	1.875	2.193
	0.2	1.384	1.189	1.106	1.058	1.040	1.037	1.084	1.284	1.607
2.0	0.01	1.963	1.787	1.720	1.652	1.575	1.513	1.451	1.429	1.527
	0.1	1.254	1.146	1.106	1.076	1.049	1.034	1.029	1.104	1.229
	0.2	1.047	0.933	0.867	0.810	0.763	0.724	0.704	0.767	0.887
	0.3	0.950	0.822	0.734	0.652	0.585	0.529	0.496	0.524	0.626
	0.4	0.885	0.744	0.639	0.539	0.455	0.388	0.347	0.340	0.412

Table 2 Dimensionless stress intensity factors for double corner cracks at a hole under remote bending, r/t=0.25

a/c	a/t	$\varphi°$ 0.1	11.3	22.5	33.8	45.0	56.3	67.5	82.5	89.9
0.2	0.01	0.991	0.989	1.220	1.436	1.639	1.847	2.053	2.341	2.482
	0.1	0.656	0.650	0.766	0.876	0.971	1.062	1.181	1.502	1.951
0.4	0.01	1.587	1.427	1.550	1.710	1.873	2.051	2.219	2.442	2.549
	0.1	1.006	0.896	0.941	1.024	1.122	1.238	1.392	1.744	2.045
	0.2	0.905	0.793	0.807	0.851	0.899	0.950	1.034	1.278	1.610
1.0	0.01	2.688	2.382	2.329	2.311	2.306	2.353	2.413	2.549	2.689
	0.1	1.857	1.632	1.584	1.578	1.604	1.674	1.781	2.026	2.224
	0.2	1.579	1.358	1.277	1.235	1.224	1.247	1.311	1.525	1.731
	0.3	1.434	1.204	1.096	1.021	0.974	0.954	0.975	1.117	1.297
	0.4	1.338	1.098	0.967	0.862	0.785	0.732	0.719	0.784	0.916
	0.5	1.259	1.009	0.860	0.732	0.629	0.552	0.512	0.505	0.569
2.0	0.01	1.900	1.725	1.653	1.578	1.493	1.423	1.354	1.320	1.406
	0.1	1.470	1.332	1.277	1.227	1.176	1.139	1.107	1.123	1.215
	0.2	1.240	1.105	1.035	0.970	0.911	0.867	0.836	0.862	0.946
	0.3	1.108	0.963	0.871	0.785	0.709	0.650	0.610	0.624	0.692
	0.4	1.017	0.859	0.746	0.640	0.548	0.476	0.425	0.418	0.464
	0.5	0.947	0.775	0.645	0.521	0.414	0.331	0.270	0.234	0.252
	0.6	0.890	0.706	0.560	0.419	0.298	0.205	0.134	0.067	0.052
	0.7	0.842	0.645	0.485	0.329	0.193	0.090	0.013	-0.084	-0.133
	0.8	0.799	0.591	0.417	0.245	0.095	-0.017	-0.102	-0.222	-0.305
	0.9	0.760	0.540	0.352	0.164	0.006	-0.118	-0.211	-0.362	-0.483

Table 3 Dimensionless stress intensity factors for double corner cracks at a hole under remote bending, r/t=0.5

a/c	a/t	$\varphi°$ 0.1	11.3	22.5	33.8	45.0	56.3	67.5	82.5	89.9
0.2	0.01	1.046	1.041	1.279	1.491	1.678	1.855	2.014	2.209	2.296
	0.1	0.724	0.713	0.848	0.971	1.081	1.190	1.319	1.605	1.873
	0.2	0.658	0.639	0.739	0.825	0.889	0.947	1.018	1.214	1.513
0.4	0.01	1.577	1.415	1.531	1.677	1.819	1.967	2.099	2.263	2.341
	0.1	1.121	0.994	1.053	1.145	1.247	1.367	1.508	1.772	1.947
	0.2	0.995	0.867	0.890	0.940	0.996	1.061	1.150	1.368	1.574
	0.3	0.925	0.793	0.791	0.809	0.828	0.851	0.898	1.046	1.233
	0.4	0.873	0.735	0.713	0.705	0.694	0.688	0.702	0.784	0.926
1.0	0.01	2.535	2.243	2.188	2.163	2.147	2.178	2.221	2.330	2.450
	0.1	2.009	1.758	1.699	1.677	1.677	1.722	1.790	1.951	2.093
	0.2	1.739	1.494	1.408	1.359	1.333	1.347	1.392	1.542	1.681
	0.3	1.582	1.330	1.216	1.134	1.077	1.054	1.065	1.172	1.292
	0.4	1.470	1.207	1.067	0.956	0.870	0.815	0.795	0.848	0.936
	0.5	1.380	1.105	0.942	0.806	0.695	0.615	0.566	0.560	0.605
	0.6	1.305	1.018	0.835	0.676	0.543	0.438	0.362	0.297	0.290
	0.7	1.239	0.940	0.739	0.559	0.403	0.275	0.175	0.056	-0.009
	0.8	1.180	0.868	0.650	0.450	0.270	0.120	0.005	-0.160	-0.283
	0.9	1.124	0.800	0.564	0.344	0.141	-0.027	-0.166	-0.389	-0.577
2.0	0.01	1.758	1.594	1.524	1.451	1.368	1.300	1.233	1.197	1.274
	0.1	1.518	1.362	1.292	1.225	1.156	1.102	1.053	1.041	1.116
	0.2	1.337	1.182	1.098	1.020	0.944	0.885	0.838	0.833	0.899
	0.3	1.212	1.048	0.945	0.849	0.759	0.689	0.637	0.627	0.679
	0.4	1.120	0.944	0.820	0.703	0.598	0.517	0.457	0.435	0.469
	0.5	1.047	0.857	0.713	0.578	0.458	0.365	0.296	0.255	0.270
	0.6	0.985	0.782	0.620	0.467	0.333	0.228	0.149	0.085	0.077
	0.7	0.931	0.715	0.536	0.366	0.218	0.101	0.013	-0.073	-0.105
	0.8	0.883	0.653	0.458	0.272	0.109	-0.018	-0.113	-0.219	-0.276
	0.9	0.839	0.595	0.385	0.182	0.007	-0.131	-0.234	-0.370	-0.455

Table 4 Dimensionless stress intensity factors for double corner cracks at a hole under remote bending, r/t=1.0

a/c	a/t	$\varphi°$ 0.1	11.3	22.5	33.8	45.0	56.3	67.5	82.5	89.9
0.2	0.01	1.059	1.059	1.296	1.497	1.668	1.826	1.957	2.109	2.186
	0.1	0.802	0.791	0.945	1.079	1.196	1.313	1.434	1.655	1.812
	0.2	0.722	0.701	0.815	0.908	0.984	1.051	1.121	1.296	1.477
	0.3	0.672	0.641	0.726	0.786	0.827	0.860	0.893	1.011	1.172
	0.4	0.632	0.592	0.654	0.685	0.696	0.701	0.709	0.777	0.893
0.4	0.01	1.546	1.386	1.496	1.632	1.759	1.891	2.003	2.138	2.203
	0.1	1.233	1.090	1.157	1.254	1.354	1.467	1.586	1.775	1.882
	0.2	1.101	0.957	0.989	1.045	1.102	1.170	1.251	1.422	1.547
	0.3	1.022	0.874	0.878	0.900	0.921	0.948	0.991	1.115	1.233
	0.4	0.961	0.807	0.787	0.780	0.771	0.767	0.778	0.852	0.946
	0.5	0.911	0.750	0.709	0.677	0.642	0.612	0.598	0.622	0.679
	0.6	0.868	0.699	0.639	0.585	0.528	0.475	0.435	0.414	0.423
	0.7	0.830	0.652	0.575	0.502	0.424	0.347	0.284	0.223	0.181
	0.8	0.795	0.609	0.516	0.425	0.324	0.224	0.144	0.053	-0.042
1.0	0.01	2.417	2.137	2.081	2.053	2.032	2.056	2.091	2.185	2.296
	0.1	2.111	1.840	1.769	1.732	1.710	1.731	1.771	1.881	1.994
	0.2	1.888	1.617	1.521	1.458	1.415	1.411	1.433	1.532	1.638
	0.3	1.733	1.455	1.332	1.238	1.166	1.131	1.127	1.197	1.286
	0.4	1.617	1.328	1.176	1.053	0.952	0.889	0.857	0.889	0.955
	0.5	1.523	1.222	1.043	0.893	0.767	0.677	0.618	0.605	0.642
	0.6	1.442	1.128	0.925	0.750	0.602	0.485	0.398	0.338	0.340
	0.7	1.370	1.042	0.818	0.621	0.449	0.306	0.193	0.087	0.051
	0.8	1.304	0.962	0.718	0.499	0.302	0.135	0.003	-0.143	-0.219
	0.9	1.242	0.887	0.622	0.380	0.160	-0.029	-0.184	-0.394	-0.516
2.0	0.01	1.660	1.504	1.436	1.365	1.285	1.219	1.154	1.119	1.190
	0.1	1.527	1.363	1.284	1.206	1.125	1.062	1.004	0.978	1.043
	0.2	1.403	1.231	1.133	1.041	0.951	0.881	0.822	0.799	0.855
	0.3	1.301	1.117	1.000	0.889	0.786	0.705	0.642	0.616	0.660
	0.4	1.217	1.019	0.881	0.751	0.632	0.541	0.473	0.440	0.470
	0.5	1.145	0.933	0.774	0.624	0.492	0.389	0.315	0.270	0.284
	0.6	1.082	0.857	0.677	0.509	0.363	0.248	0.164	0.105	0.103
	0.7	1.026	0.787	0.587	0.402	0.241	0.114	0.021	-0.053	-0.073
	0.8	0.976	0.722	0.504	0.301	0.125	-0.014	-0.113	-0.201	-0.239
	0.9	0.929	0.660	0.424	0.203	0.013	-0.137	-0.245	-0.362	-0.421

Table 5 Dimensionless stress intensity factors for double corner cracks at a hole under remote bending, r/t=1.5

a/c	a/t	$\varphi°$ 0.1	11.3	22.5	33.8	45.0	56.3	67.5	82.5	89.9
0.2	0.01	1.062	1.062	1.298	1.495	1.660	1.811	1.932	2.069	2.138
	0.1	0.849	0.836	1.002	1.142	1.264	1.383	1.500	1.687	1.804
	0.2	0.768	0.744	0.869	0.967	1.044	1.115	1.188	1.345	1.481
	0.3	0.714	0.681	0.774	0.838	0.881	0.915	0.950	1.059	1.184
	0.4	0.671	0.629	0.696	0.729	0.741	0.747	0.755	0.819	0.912
	0.5	0.636	0.585	0.627	0.635	0.620	0.602	0.588	0.611	0.660
	0.6	0.606	0.545	0.566	0.550	0.513	0.472	0.436	0.421	0.418
0.4	0.01	1.502	1.368	1.475	1.599	1.720	1.850	1.959	2.100	2.195
	0.1	1.269	1.138	1.208	1.298	1.392	1.500	1.603	1.762	1.868
	0.2	1.138	1.003	1.038	1.089	1.144	1.209	1.279	1.418	1.525
	0.3	1.055	0.913	0.918	0.935	0.952	0.976	1.009	1.108	1.202
	0.4	0.992	0.841	0.820	0.807	0.791	0.782	0.783	0.837	0.905
	0.5	0.937	0.778	0.735	0.695	0.651	0.614	0.586	0.594	0.629
	0.6	0.889	0.722	0.658	0.594	0.526	0.462	0.407	0.369	0.363
	0.7	0.846	0.671	0.587	0.502	0.409	0.318	0.237	0.159	0.110
	0.8	0.807	0.623	0.521	0.415	0.296	0.179	0.079	-0.035	-0.128
	0.9	0.771	0.578	0.458	0.331	0.187	0.046	-0.079	-0.250	-0.389
1.0	0.01	2.368	2.093	2.037	2.009	1.987	2.008	2.040	2.130	2.236
	0.1	2.151	1.872	1.796	1.751	1.720	1.731	1.759	1.850	1.952
	0.2	1.966	1.681	1.579	1.507	1.453	1.439	1.449	1.526	1.619
	0.3	1.821	1.528	1.396	1.295	1.213	1.170	1.156	1.208	1.286
	0.4	1.705	1.400	1.239	1.108	0.998	0.928	0.890	0.910	0.968
	0.5	1.609	1.291	1.102	0.942	0.808	0.712	0.648	0.631	0.665
	0.6	1.526	1.193	0.979	0.794	0.637	0.514	0.422	0.363	0.371
	0.7	1.451	1.105	0.866	0.658	0.476	0.326	0.208	0.109	0.087
	0.8	1.384	1.022	0.761	0.529	0.322	0.146	0.008	-0.127	-0.181
	0.9	1.320	0.944	0.660	0.404	0.172	-0.027	-0.190	-0.390	-0.481
2.0	0.01	1.622	1.469	1.402	1.332	1.253	1.188	1.124	1.089	1.158
	0.1	1.527	1.360	1.276	1.195	1.110	1.043	0.982	0.951	1.013
	0.2	1.429	1.250	1.147	1.048	0.952	0.876	0.813	0.783	0.835
	0.3	1.343	1.150	1.025	0.907	0.796	0.709	0.642	0.609	0.650
	0.4	1.267	1.059	0.911	0.773	0.648	0.551	0.479	0.440	0.469
	0.5	1.200	0.976	0.806	0.648	0.509	0.401	0.323	0.276	0.291
	0.6	1.139	0.900	0.708	0.532	0.379	0.259	0.173	0.115	0.116
	0.7	1.083	0.829	0.617	0.423	0.255	0.122	0.028	-0.041	-0.055
	0.8	1.032	0.762	0.531	0.319	0.135	-0.010	-0.110	-0.190	-0.219
	0.9	0.984	0.698	0.448	0.217	0.018	-0.138	-0.249	-0.354	-0.402

Table 6 Dimensionless stress intensity factors for double corner cracks at a hole under remote bending, r/t=2.5

a/c	a/t	$\varphi°$ 0.1	11.3	22.5	33.8	45.0	56.3	67.5	82.5	89.9
0.2	0.01	1.056	1.055	1.288	1.481	1.640	1.783	1.896	2.020	2.082
	0.1	0.901	0.887	1.064	1.211	1.334	1.452	1.558	1.705	1.789
	0.2	0.819	0.793	0.928	1.032	1.113	1.188	1.260	1.391	1.484
	0.3	0.764	0.728	0.830	0.898	0.941	0.977	1.014	1.110	1.196
	0.4	0.720	0.674	0.747	0.783	0.794	0.799	0.808	0.866	0.934
	0.5	0.682	0.626	0.673	0.681	0.665	0.645	0.630	0.649	0.690
	0.6	0.649	0.584	0.607	0.590	0.551	0.506	0.467	0.449	0.454
	0.7	0.620	0.545	0.547	0.508	0.445	0.375	0.313	0.262	0.229
	0.8	0.594	0.510	0.491	0.431	0 345	0.251	0.170	0.092	0.021
	0.9	0.570	0.477	0.437	0.359	0.249	0.134	0.034	-0.097	-0.211
0.4	0.01	1.475	1.344	1.448	1.568	1.684	1.809	1.912	2.045	2.136
	0.1	1.322	1.185	1.256	1.344	1.434	1.534	1.623	1.754	1.844
	0.2	1.206	1.062	1.101	1.153	1.206	1.268	1.329	1.440	1.525
	0.3	1.122	0.970	0.978	0.996	1.011	1.036	1.064	1.145	1.218
	0.4	1.056	0.896	0.875	0.861	0.843	0.834	0.832	0.877	0.932
	0.5	1.001	0.831	0.785	0.742	0.695	0.656	0.626	0.632	0.664
	0.6	0.951	0.772	0.704	0.635	0.562	0.495	0.436	0.400	0.405
	0.7	0.907	0.719	0.629	0.537	0.438	0.341	0.255	0.181	0.156
	0.8	0.866	0.668	0.558	0.444	0.319	0.193	0.085	-0.023	-0.078
	0.9	0.827	0.620	0.490	0.354	0.201	0.051	-0.083	-0.252	-0.343
1.0	0.01	2.240	2.033	1.983	1.949	1.933	1.958	1.984	2.088	2.231
	0.1	2.102	1.874	1.795	1.737	1.700	1.705	1.717	1.806	1.933
	0.2	1.965	1.718	1.607	1.518	1.452	1.426	1.416	1.480	1.587
	0.3	1.846	1.579	1.435	1.313	1.214	1.157	1.122	1.156	1.240
	0.4	1.742	1.455	1.277	1.122	0.993	0.905	0.845	0.846	0.906
	0.5	1.651	1.343	1.132	0.946	0.788	0.670	0.584	0.548	0.581
	0.6	1.570	1.241	0.999	0.783	0.597	0.449	0.333	0.257	0.262
	0.7	1.496	1.146	0.875	0.630	0.415	0.235	0.091	-0.024	-0.049
	0.8	1.427	1.057	0.758	0.485	0.239	0.029	-0.140	-0.293	-0.347
	0.9	1.363	0.972	0.643	0.342	0.066	-0.175	-0.374	-0.596	-0.687
2.0	0.01	1.579	1.429	1.364	1.295	1.217	1.154	1.092	1.057	1.123
	0.1	1.513	1.345	1.260	1.176	1.088	1.018	0.956	0.922	0.980
	0.2	1.441	1.256	1.149	1.045	0.944	0.863	0.796	0.761	0.809
	0.3	1.373	1.171	1.040	0.915	0.798	0.707	0.635	0.597	0.635
	0.4	1.309	1.091	0.935	0.789	0.657	0.555	0.479	0.437	0.464
	0.5	1.250	1.014	0.834	0.668	0.522	0.410	0.328	0.280	0.295
	0.6	1.195	0.942	0.739	0.554	0.393	0.269	0.181	0.125	0.128
	0.7	1.142	0.872	0.648	0.444	0.268	0.131	0.036	-0.027	-0.037
	0.8	1.093	0.806	0.560	0.337	0.145	-0.005	-0.105	-0.174	-0.196
	0.9	1.045	0.741	0.474	0.231	0.024	-0.137	-0.248	-0.341	-0.379

Table 7 Dimensionless stress intensity factors for double corner cracks at a hole under remote tension, r/t=0.1

a/c	a/t	$\varphi°$ 0.1	11.3	22.5	33.8	45.0	56.3	67.5	82.5	89.9
0.2	0.01	0.827	0.836	1.033	1.232	1.440	1.677	1.954	2.448	2.758
0.4	0.01	1.452	1.314	1.442	1.621	1.824	2.060	2.313	2.697	2.895
1.0	0.01	2.791	2.487	2.454	2.467	2.501	2.594	2.707	2.925	3.112
	0.1	1.629	1.467	1.448	1.483	1.563	1.677	1.850	2.301	2.713
	0.2	1.473	1.320	1.283	1.293	1.339	1.396	1.513	1.874	2.402
2.0	0.01	2.082	1.901	1.837	1.771	1.694	1.632	1.569	1.548	1.655
	0.1	1.327	1.248	1.241	1.242	1.243	1.250	1.265	1.378	1.540
	0.2	1.125	1.055	1.035	1.025	1.021	1.017	1.028	1.168	1.370
	0.3	1.048	0.975	0.942	0.922	0.912	0.898	0.904	1.037	1.271
	0.4	1.005	0.929	0.891	0.867	0.854	0.832	0.833	0.946	1.202

Table 8 Dimensionless stress intensity factors for double corner cracks at a hole under remote tension, r/t=0.25

a/c	a/t	$\varphi°$ 0.1	11.3	22.5	33.8	45.0	56.3	67.5	82.5	89.9
0.2	0.01	1.093	1.094	1.357	1.610	1.856	2.114	2.376	2.746	2.926
	0.1	0.651	0.661	0.793	0.932	1.063	1.197	1.383	1.901	2.585
0.4	0.01	1.810	1.631	1.778	1.971	2.171	2.390	2.599	2.877	3.010
	0.1	1.026	0.936	1.009	1.134	1.290	1.477	1.727	2.282	2.730
	0.2	0.938	0.859	0.910	1.011	1.129	1.258	1.444	1.932	2.550
1.0	0.01	3.122	2.771	2.717	2.705	2.707	2.769	2.846	3.014	3.181
	0.1	2.056	1.851	1.852	1.906	2.000	2.150	2.343	2.730	3.014
	0.2	1.734	1.562	1.552	1.595	1.681	1.809	1.995	2.445	2.823
	0.3	1.602	1.439	1.416	1.444	1.515	1.614	1.774	2.217	2.665
	0.4	1.536	1.378	1.345	1.360	1.419	1.499	1.642	2.059	2.562
	0.5	1.493	1.338	1.302	1.314	1.367	1.436	1.571	1.957	2.506
2.0	0.01	2.217	2.017	1.938	1.855	1.759	1.681	1.602	1.565	1.667
	0.1	1.696	1.577	1.559	1.545	1.523	1.512	1.497	1.543	1.674
	0.2	1.426	1.342	1.337	1.336	1.333	1.338	1.346	1.442	1.597
	0.3	1.284	1.211	1.202	1.200	1.198	1.202	1.217	1.342	1.515
	0.4	1.199	1.128	1.113	1.106	1.105	1.107	1.125	1.267	1.458
	0.5	1.144	1.073	1.052	1.042	1.043	1.044	1.063	1.212	1.421
	0.6	1.107	1.035	1.010	1.000	1.003	1.003	1.021	1.171	1.396
	0.7	1.082	1.010	0.984	0.974	0.979	0.978	0.996	1.144	1.384
	0.8	1.068	0.995	0.969	0.962	0.969	0.970	0.994	1.148	1.410
	0.9	1.061	0.987	0.966	0.965	0.978	0.986	1.031	1.188	1.483

Table 9 Dimensionless stress intensity factors for double corner cracks at a hole under remote tension, r/t=0.5

a/c	a/t	$\varphi°$ 0.1	11.3	22.5	33.8	45.0	56.3	67.5	82.5	89.9
0.2	0.01	1.329	1.325	1.636	1.919	2.175	2.425	2.654	2.939	3.066
	0.1	0.748	0.753	0.917	1.089	1.264	1.462	1.718	2.292	2.772
	0.2	0.671	0.680	0.817	0.962	1.098	1.239	1.431	1.946	2.618
0.4	0.01	2.054	1.846	2.003	2.202	2.397	2.604	2.789	3.021	3.131
	0.1	1.272	1.151	1.258	1.418	1.609	1.841	2.116	2.607	2.906
	0.2	1.078	0.979	1.055	1.183	1.340	1.528	1.777	2.321	2.763
	0.3	1.003	0.914	0.974	1.085	1.219	1.375	1.591	2.117	2.657
	0.4	0.963	0.881	0.933	1.035	1.157	1.293	1.489	1.982	2.595
1.0	0.01	3.345	2.964	2.897	2.871	2.857	2.905	2.968	3.119	3.282
	0.1	2.552	2.278	2.263	2.300	2.367	2.495	2.650	2.944	3.171
	0.2	2.148	1.925	1.920	1.968	2.053	2.196	2.382	2.761	3.044
	0.3	1.936	1.737	1.726	1.769	1.854	1.988	2.178	2.602	2.934
	0.4	1.808	1.621	1.603	1.639	1.720	1.847	2.034	2.484	2.862
	0.5	1.724	1.544	1.520	1.553	1.635	1.757	1.942	2.406	2.825
	0.6	1.669	1.495	1.467	1.499	1.585	1.706	1.888	2.355	2.814
	0.7	1.636	1.465	1.437	1.473	1.564	1.683	1.867	2.338	2.838
	0.8	1.622	1.453	1.427	1.469	1.570	1.694	1.899	2.401	2.956
	0.9	1.627	1.457	1.439	1.495	1.614	1.767	2.042	2.606	3.242
2.0	0.01	2.328	2.114	2.026	1.933	1.826	1.739	1.652	1.607	1.709
	0.1	1.998	1.833	1.786	1.740	1.684	1.643	1.597	1.600	1.719
	0.2	1.755	1.626	1.602	1.581	1.551	1.533	1.514	1.555	1.687
	0.3	1.592	1.484	1.468	1.456	1.440	1.434	1.430	1.501	1.645
	0.4	1.480	1.383	1.368	1.360	1.351	1.352	1.360	1.457	1.611
	0.5	1.399	1.308	1.293	1.286	1.284	1.291	1.308	1.423	1.589
	0.6	1.339	1.253	1.237	1.233	1.236	1.247	1.268	1.398	1.575
	0.7	1.294	1.212	1.196	1.195	1.204	1.217	1.240	1.383	1.573
	0.8	1.263	1.182	1.168	1.171	1.186	1.202	1.234	1.400	1.606
	0.9	1.244	1.164	1.153	1.163	1.187	1.216	1.272	1.466	1.696

Table 10 Dimensionless stress intensity factors for double corner cracks at a hole under remote tension, r/t=1.0

a/c	a/t	$\varphi°$ 0.1	11.3	22.5	33.8	45.0	56.3	67.5	82.5	89.9
0.2	0.01	1.552	1.545	1.898	2.208	2.474	2.719	2.927	3.163	3.263
	0.1	0.942	0.943	1.164	1.387	1.617	1.875	2.175	2.700	3.016
	0.2	0.779	0.782	0.954	1.133	1.317	1.525	1.793	2.382	2.862
	0.3	0.715	0.722	0.872	1.029	1.186	1.357	1.589	2.163	2.758
	0.4	0.682	0.691	0.830	0.977	1.119	1.271	1.479	2.022	2.703
0.4	0.01	2.286	2.052	2.220	2.428	2.625	2.829	3.004	3.216	3.317
	0.1	1.643	1.479	1.616	1.809	2.024	2.273	2.537	2.932	3.137
	0.2	1.349	1.217	1.327	1.493	1.689	1.926	2.206	2.700	2.999
	0.3	1.203	1.088	1.179	1.323	1.499	1.713	1.984	2.524	2.901
	0.4	1.117	1.014	1.090	1.220	1.382	1.580	1.842	2.404	2.850
	0.5	1.065	0.968	1.035	1.157	1.314	1.505	1.762	2.336	2.844
	0.6	1.032	0.941	1.002	1.123	1.281	1.472	1.728	2.308	2.874
	0.7	1.013	0.926	0.986	1.111	1.278	1.472	1.737	2.331	2.957
	0.8	1.003	0.920	0.982	1.118	1.301	1.512	1.815	2.473	3.180
1.0	0.01	3.601	3.188	3.110	3.074	3.050	3.091	3.148	3.294	3.461
	0.1	3.092	2.740	2.696	2.703	2.733	2.827	2.942	3.169	3.367
	0.2	2.710	2.408	2.384	2.413	2.472	2.594	2.745	3.037	3.267
	0.3	2.448	2.181	2.164	2.200	2.272	2.406	2.579	2.922	3.180
	0.4	2.265	2.020	2.003	2.041	2.121	2.263	2.454	2.841	3.128
	0.5	2.133	1.903	1.885	1.925	2.014	2.165	2.370	2.795	3.113
	0.6	2.036	1.819	1.801	1.845	1.945	2.105	2.319	2.775	3.124
	0.7	1.967	1.759	1.743	1.795	1.908	2.074	2.299	2.792	3.175
	0.8	1.924	1.722	1.709	1.772	1.901	2.082	2.340	2.907	3.342
	0.9	1.910	1.709	1.702	1.783	1.940	2.165	2.514	3.211	3.723
2.0	0.01	2.478	2.249	2.151	2.049	1.932	1.836	1.741	1.689	1.796
	0.1	2.288	2.080	2.004	1.928	1.840	1.771	1.700	1.674	1.788
	0.2	2.112	1.928	1.871	1.815	1.750	1.699	1.647	1.645	1.766
	0.3	1.968	1.804	1.759	1.717	1.666	1.630	1.593	1.614	1.741
	0.4	1.852	1.703	1.665	1.632	1.594	1.571	1.549	1.591	1.725
	0.5	1.759	1.620	1.587	1.562	1.536	1.526	1.517	1.578	1.719
	0.6	1.682	1.554	1.526	1.508	1.493	1.493	1.494	1.571	1.720
	0.7	1.621	1.501	1.478	1.468	1.463	1.471	1.480	1.575	1.734
	0.8	1.575	1.462	1.443	1.441	1.447	1.464	1.489	1.617	1.792
	0.9	1.545	1.436	1.423	1.431	1.453	1.493	1.554	1.730	1.927

Table 11 Dimensionless stress intensity factors for double corner cracks at a hole under remote tension, r/t=1.5

a/c	a/t	$\varphi°$ 0.1	11.3	22.5	33.8	45.0	56.3	67.5	82.5	89.9
0.2	0.01	1.642	1.633	2.004	2.324	2.593	2.836	3.036	3.255	3.346
	0.1	1.089	1.087	1.346	1.600	1.855	2.132	2.432	2.896	3.141
	0.2	0.879	0.880	1.083	1.290	1.505	1.750	2.048	2.617	2.995
	0.3	0.784	0.788	0.962	1.142	1.328	1.539	1.813	2.412	2.893
	0.4	0.734	0.740	0.896	1.061	1.228	1.418	1.674	2.276	2.843
	0.5	0.705	0.713	0.859	1.015	1.175	1.357	1.603	2.201	2.844
	0.6	0.685	0.695	0.836	0.992	1.155	1.337	1.582	2.176	2.888
0.4	0.01	2.378	2.133	2.305	2.518	2.716	2.920	3.092	3.297	3.396
	0.1	1.861	1.671	1.822	2.026	2.245	2.491	2.737	3.080	3.249
	0.2	1.551	1.395	1.525	1.710	1.922	2.172	2.448	2.886	3.124
	0.3	1.371	1.236	1.348	1.514	1.711	1.950	2.233	2.732	3.031
	0.4	1.258	1.137	1.233	1.385	1.570	1.800	2.086	2.629	2.985
	0.5	1.182	1.071	1.157	1.299	1.481	1.708	1.999	2.578	2.990
	0.6	1.131	1.027	1.106	1.246	1.432	1.662	1.959	2.568	3.034
	0.7	1.099	1.000	1.075	1.219	1.415	1.653	1.963	2.612	3.137
	0.8	1.082	0.988	1.062	1.216	1.428	1.686	2.044	2.789	3.397
	0.9	1.083	0.993	1.069	1.241	1.486	1.804	2.294	3.242	3.986
1.0	0.01	3.704	3.279	3.197	3.158	3.129	3.168	3.224	3.369	3.538
	0.1	3.334	2.949	2.891	2.882	2.894	2.972	3.068	3.269	3.458
	0.2	3.014	2.670	2.631	2.644	2.683	2.785	2.912	3.162	3.372
	0.3	2.766	2.456	2.427	2.451	2.506	2.625	2.775	3.069	3.299
	0.4	2.575	2.289	2.265	2.296	2.363	2.498	2.671	3.008	3.260
	0.5	2.428	2.161	2.139	2.176	2.258	2.410	2.605	2.983	3.259
	0.6	2.315	2.063	2.045	2.090	2.189	2.357	2.570	2.985	3.286
	0.7	2.229	1.990	1.977	2.034	2.151	2.334	2.566	3.028	3.360
	0.8	2.173	1.943	1.934	2.006	2.144	2.350	2.628	3.183	3.565
	0.9	2.148	1.922	1.923	2.014	2.188	2.451	2.839	3.556	4.017
2.0	0.01	2.541	2.305	2.204	2.098	1.977	1.877	1.779	1.725	1.834
	0.1	2.407	2.183	2.096	2.008	1.907	1.826	1.745	1.709	1.822
	0.2	2.273	2.066	1.993	1.921	1.837	1.771	1.703	1.684	1.801
	0.3	2.155	1.964	1.902	1.842	1.771	1.717	1.662	1.660	1.781
	0.4	2.054	1.876	1.821	1.770	1.712	1.671	1.630	1.645	1.772
	0.5	1.968	1.801	1.753	1.710	1.665	1.638	1.610	1.642	1.774
	0.6	1.894	1.738	1.696	1.663	1.632	1.617	1.599	1.645	1.785
	0.7	1.832	1.686	1.651	1.629	1.610	1.605	1.598	1.663	1.810
	0.8	1.785	1.647	1.619	1.607	1.602	1.611	1.623	1.724	1.887
	0.9	1.754	1.620	1.601	1.603	1.617	1.655	1.711	1.865	2.053

Table 12 Dimensionless stress intensity factors for double corner cracks at a hole under remote tension, r/t=2.5

a/c	a/t	$\varphi°$ 0.1	11.3	22.5	33.8	45.0	56.3	67.5	82.5	89.9
0.2	0.01	1.715	1.705	2.089	2.417	2.688	2.929	3.122	3.326	3.411
	0.1	1.280	1.274	1.576	1.861	2.134	2.415	2.694	3.078	3.260
	0.2	1.042	1.040	1.287	1.532	1.781	2.056	2.362	2.860	3.136
	0.3	0.913	0.914	1.127	1.342	1.566	1.821	2.127	2.689	3.045
	0.4	0.836	0.839	1.029	1.224	1.429	1.668	1.971	2.577	3.006
	0.5	0.786	0.791	0.965	1.149	1.346	1.580	1.883	2.523	3.022
	0.6	0.754	0.761	0.924	1.104	1.304	1.539	1.848	2.517	3.085
	0.7	0.733	0.742	0.900	1.083	1.292	1.537	1.861	2.576	3.218
	0.8	0.723	0.734	0.890	1.084	1.310	1.578	1.956	2.785	3.536
	0.9	0.721	0.738	0.894	1.109	1.368	1.704	2.234	3.322	4.258
0.4	0.01	2.449	2.197	2.372	2.588	2.787	2.990	3.160	3.361	3.457
	0.1	2.086	1.869	2.032	2.244	2.461	2.698	2.920	3.211	3.350
	0.2	1.810	1.624	1.773	1.975	2.195	2.445	2.700	3.067	3.251
	0.3	1.618	1.455	1.590	1.779	1.993	2.246	2.520	2.947	3.172
	0.4	1.482	1.335	1.457	1.634	1.844	2.099	2.391	2.873	3.140
	0.5	1.383	1.248	1.360	1.530	1.740	2.003	2.315	2.849	3.160
	0.6	1.312	1.186	1.291	1.459	1.678	1.952	2.283	2.869	3.224
	0.7	1.262	1.143	1.244	1.417	1.650	1.940	2.296	2.949	3.357
	0.8	1.230	1.117	1.217	1.401	1.655	1.974	2.393	3.182	3.670
	0.9	1.219	1.112	1.213	1.418	1.711	2.105	2.683	3.740	4.361
1.0	0.01	3.784	3.348	3.264	3.222	3.191	3.228	3.282	3.427	3.598
	0.1	3.545	3.130	3.060	3.039	3.034	3.096	3.176	3.355	3.537
	0.2	3.312	2.927	2.873	2.868	2.884	2.965	3.066	3.277	3.471
	0.3	3.112	2.755	2.711	2.718	2.748	2.844	2.966	3.209	3.416
	0.4	2.944	2.609	2.572	2.588	2.633	2.748	2.894	3.173	3.395
	0.5	2.805	2.489	2.458	2.483	2.547	2.686	2.858	3.175	3.415
	0.6	2.690	2.392	2.367	2.405	2.493	2.656	2.851	3.207	3.467
	0.7	2.600	2.316	2.300	2.355	2.467	2.654	2.877	3.285	3.573
	0.8	2.536	2.264	2.257	2.332	2.474	2.694	2.976	3.493	3.829
	0.9	2.507	2.240	2.246	2.347	2.534	2.829	3.246	3.953	4.372
2.0	0.01	2.588	2.347	2.244	2.136	2.011	1.910	1.809	1.753	1.864
	0.1	2.505	2.268	2.172	2.075	1.963	1.873	1.783	1.739	1.851
	0.2	2.414	2.188	2.103	2.016	1.915	1.834	1.753	1.719	1.834
	0.3	2.329	2.115	2.037	1.959	1.868	1.796	1.724	1.702	1.819
	0.4	2.253	2.049	1.977	1.907	1.826	1.765	1.705	1.696	1.816
	0.5	2.186	1.990	1.925	1.863	1.795	1.747	1.699	1.702	1.827
	0.6	2.126	1.941	1.882	1.830	1.776	1.742	1.702	1.718	1.849
	0.7	2.075	1.899	1.849	1.809	1.769	1.746	1.717	1.750	1.889
	0.8	2.036	1.868	1.826	1.799	1.775	1.769	1.763	1.832	1.987
	0.9	2.013	1.850	1.819	1.807	1.808	1.836	1.880	2.005	2.187

Table 13 Dimensionless stress intensity factors for double corner cracks at a hole under wedge loading, r/t=0.1

a/c	a/t	$\varphi°$ 0.1	11.3	22.5	33.8	45.0	56.3	67.5	82.5	89.9
0.2	0.01	0.232	0.238	0.300	0.378	0.471	0.590	0.752	1.100	1.373
0.4	0.01	0.529	0.482	0.536	0.618	0.721	0.850	1.007	1.285	1.451
1.0	0.01	1.228	1.098	1.094	1.116	1.153	1.223	1.309	1.468	1.588
	0.1	0.403	0.374	0.382	0.418	0.484	0.566	0.692	0.984	1.308
	0.2	0.244	0.226	0.223	0.244	0.291	0.344	0.439	0.699	1.095
2.0	0.01	0.993	0.909	0.884	0.861	0.833	0.813	0.792	0.796	0.857
	0.1	0.461	0.445	0.457	0.474	0.496	0.519	0.550	0.651	0.771
	0.2	0.306	0.297	0.303	0.316	0.338	0.359	0.394	0.500	0.657
	0.3	0.233	0.225	0.223	0.232	0.254	0.273	0.308	0.416	0.598
	0.4	0.191	0.182	0.177	0.185	0.205	0.220	0.253	0.359	0.554

Table 14 Dimensionless stress intensity factors for double corner cracks at a hole under wedge loading, r/t=0.25

a/c	a/t	$\varphi°$ 0.1	11.3	22.5	33.8	45.0	56.3	67.5	82.5	89.9
0.2	0.01	0.402	0.405	0.508	0.617	0.735	0.873	1.034	1.305	1.457
	0.1	0.066	0.077	0.088	0.118	0.163	0.227	0.343	0.697	1.222
0.4	0.01	0.763	0.690	0.760	0.856	0.963	1.089	1.221	1.415	1.513
	0.1	0.214	0.205	0.225	0.275	0.351	0.453	0.607	0.964	1.331
	0.2	0.118	0.120	0.124	0.152	0.203	0.270	0.389	0.722	1.191
1.0	0.01	1.474	1.311	1.293	1.297	1.311	1.357	1.413	1.521	1.617
	0.1	0.719	0.658	0.675	0.719	0.790	0.888	1.021	1.301	1.520
	0.2	0.487	0.449	0.461	0.501	0.570	0.657	0.786	1.083	1.380
	0.3	0.367	0.340	0.345	0.377	0.439	0.514	0.635	0.919	1.264
	0.4	0.300	0.278	0.277	0.301	0.356	0.421	0.532	0.809	1.191
	0.5	0.257	0.238	0.233	0.254	0.303	0.360	0.462	0.735	1.146
2.0	0.01	1.090	0.993	0.958	0.922	0.879	0.846	0.812	0.799	0.854
	0.1	0.692	0.656	0.665	0.677	0.687	0.702	0.718	0.779	0.867
	0.2	0.522	0.506	0.519	0.536	0.555	0.576	0.603	0.696	0.807
	0.3	0.427	0.416	0.427	0.442	0.462	0.484	0.515	0.618	0.748
	0.4	0.363	0.353	0.360	0.375	0.396	0.418	0.453	0.563	0.710
	0.5	0.316	0.307	0.311	0.324	0.348	0.372	0.410	0.522	0.685
	0.6	0.281	0.273	0.274	0.287	0.313	0.337	0.377	0.488	0.664
	0.7	0.256	0.247	0.247	0.260	0.286	0.310	0.352	0.462	0.649
	0.8	0.237	0.227	0.227	0.241	0.267	0.291	0.336	0.451	0.655
	0.9	0.223	0.213	0.213	0.229	0.256	0.281	0.333	0.451	0.686

Table 15 Dimensionless stress intensity factors for double corner cracks at a hole under wedge loading, r/t=0.5

a/c	a/t	$\varphi°$ 0.1	11.3	22.5	33.8	45.0	56.3	67.5	82.5	89.9
0.2	0.01	0.564	0.564	0.702	0.836	0.968	1.107	1.249	1.450	1.547
	0.1	0.159	0.166	0.206	0.265	0.341	0.442	0.596	0.968	1.364
	0.2	0.082	0.093	0.108	0.143	0.191	0.259	0.380	0.733	1.249
0.4	0.01	0.949	0.855	0.933	1.035	1.141	1.258	1.369	1.518	1.589
	0.1	0.406	0.373	0.414	0.485	0.581	0.704	0.869	1.209	1.462
	0.2	0.251	0.236	0.258	0.310	0.388	0.490	0.645	0.998	1.357
	0.3	0.179	0.173	0.184	0.222	0.285	0.370	0.510	0.853	1.273
	0.4	0.141	0.139	0.144	0.174	0.226	0.296	0.420	0.756	1.219
1.0	0.01	1.643	1.459	1.430	1.424	1.424	1.457	1.499	1.588	1.676
	0.1	1.039	0.938	0.948	0.986	1.045	1.137	1.252	1.472	1.631
	0.2	0.783	0.711	0.724	0.765	0.832	0.927	1.055	1.329	1.543
	0.3	0.638	0.581	0.591	0.630	0.696	0.786	0.914	1.205	1.462
	0.4	0.540	0.492	0.498	0.534	0.600	0.686	0.815	1.112	1.406
	0.5	0.468	0.427	0.431	0.464	0.530	0.614	0.744	1.044	1.371
	0.6	0.416	0.380	0.380	0.412	0.478	0.561	0.691	0.991	1.347
	0.7	0.378	0.345	0.344	0.375	0.441	0.521	0.652	0.955	1.337
	0.8	0.352	0.320	0.319	0.350	0.417	0.495	0.632	0.950	1.370
	0.9	0.336	0.305	0.304	0.338	0.408	0.491	0.649	0.993	1.473
2.0	0.01	1.166	1.061	1.019	0.976	0.925	0.884	0.842	0.823	0.876
	0.1	0.900	0.837	0.830	0.824	0.814	0.810	0.804	0.830	0.902
	0.2	0.735	0.696	0.701	0.707	0.712	0.722	0.733	0.789	0.877
	0.3	0.632	0.603	0.610	0.621	0.631	0.647	0.667	0.744	0.843
	0.4	0.561	0.536	0.543	0.555	0.570	0.589	0.615	0.707	0.817
	0.5	0.507	0.485	0.492	0.504	0.523	0.545	0.576	0.678	0.800
	0.6	0.465	0.445	0.451	0.465	0.486	0.511	0.545	0.653	0.785
	0.7	0.431	0.412	0.418	0.434	0.458	0.484	0.521	0.633	0.776
	0.8	0.403	0.386	0.392	0.409	0.436	0.464	0.506	0.627	0.784
	0.9	0.382	0.365	0.372	0.392	0.423	0.455	0.510	0.640	0.819

Table 16 Dimensionless stress intensity factors for double corner cracks at a hole under wedge loading, r/t=1.0

a/c	a/t	$\varphi°$ 0.1	11.3	22.5	33.8	45.0	56.3	67.5	82.5	89.9
0.2	0.01	0.723	0.721	0.890	1.044	1.184	1.320	1.444	1.598	1.667
	0.1	0.307	0.311	0.388	0.479	0.585	0.715	0.888	1.248	1.522
	0.2	0.178	0.185	0.229	0.292	0.374	0.482	0.644	1.023	1.419
	0.3	0.119	0.128	0.154	0.201	0.265	0.354	0.500	0.874	1.342
	0.4	0.089	0.100	0.116	0.152	0.204	0.276	0.405	0.775	1.295
0.4	0.01	1.117	1.003	1.089	1.197	1.303	1.415	1.515	1.640	1.700
	0.1	0.642	0.581	0.642	0.733	0.845	0.984	1.149	1.435	1.604
	0.2	0.456	0.415	0.458	0.532	0.631	0.757	0.925	1.266	1.518
	0.3	0.348	0.320	0.351	0.414	0.502	0.618	0.781	1.136	1.449
	0.4	0.277	0.258	0.280	0.334	0.414	0.521	0.682	1.043	1.405
	0.5	0.228	0.216	0.232	0.278	0.353	0.454	0.613	0.979	1.384
	0.6	0.196	0.188	0.199	0.240	0.311	0.407	0.564	0.936	1.378
	0.7	0.174	0.169	0.176	0.215	0.283	0.376	0.532	0.914	1.394
	0.8	0.158	0.155	0.161	0.199	0.268	0.360	0.523	0.936	1.468
1.0	0.01	1.815	1.608	1.572	1.558	1.549	1.575	1.610	1.691	1.780
	0.1	1.394	1.244	1.238	1.259	1.297	1.370	1.458	1.623	1.750
	0.2	1.136	1.018	1.022	1.055	1.108	1.196	1.309	1.528	1.689
	0.3	0.973	0.874	0.879	0.914	0.973	1.065	1.187	1.440	1.630
	0.4	0.858	0.771	0.775	0.811	0.873	0.966	1.095	1.373	1.591
	0.5	0.770	0.692	0.696	0.732	0.798	0.895	1.030	1.326	1.570
	0.6	0.701	0.631	0.635	0.672	0.743	0.842	0.982	1.291	1.560
	0.7	0.646	0.582	0.586	0.627	0.703	0.804	0.950	1.273	1.569
	0.8	0.604	0.545	0.550	0.594	0.676	0.782	0.943	1.296	1.629
	0.9	0.576	0.519	0.526	0.576	0.668	0.789	0.989	1.394	1.782
2.0	0.01	1.261	1.145	1.098	1.047	0.989	0.942	0.895	0.870	0.926
	0.1	1.101	1.009	0.982	0.956	0.924	0.901	0.875	0.877	0.942
	0.2	0.969	0.896	0.883	0.870	0.853	0.844	0.834	0.856	0.930
	0.3	0.870	0.810	0.803	0.798	0.790	0.789	0.790	0.831	0.912
	0.4	0.795	0.742	0.738	0.737	0.736	0.743	0.753	0.810	0.898
	0.5	0.736	0.688	0.686	0.689	0.694	0.707	0.724	0.794	0.890
	0.6	0.688	0.645	0.644	0.650	0.660	0.678	0.701	0.782	0.885
	0.7	0.648	0.609	0.610	0.619	0.635	0.656	0.682	0.774	0.885
	0.8	0.617	0.581	0.583	0.596	0.616	0.641	0.675	0.784	0.906
	0.9	0.594	0.559	0.564	0.581	0.608	0.642	0.693	0.824	0.962

Table 17 Dimensionless stress intensity factors for double corner cracks at a hole under wedge loading, r/t=1.5

a/c	a/t	$\varphi°$ 0.1	11.3	22.5	33.8	45.0	56.3	67.5	82.5	89.9
0.2	0.01	0.797	0.794	0.978	1.140	1.283	1.416	1.533	1.669	1.729
	0.1	0.405	0.407	0.508	0.617	0.739	0.883	1.060	1.390	1.602
	0.2	0.261	0.265	0.331	0.413	0.513	0.639	0.812	1.189	1.513
	0.3	0.182	0.189	0.234	0.299	0.383	0.494	0.659	1.045	1.443
	0.4	0.136	0.145	0.176	0.228	0.300	0.399	0.556	0.944	1.398
	0.5	0.108	0.119	0.141	0.184	0.247	0.336	0.486	0.878	1.378
	0.6	0.090	0.102	0.118	0.156	0.213	0.295	0.438	0.835	1.379
0.4	0.01	1.193	1.071	1.160	1.271	1.377	1.487	1.584	1.702	1.758
	0.1	0.785	0.707	0.778	0.879	0.997	1.137	1.294	1.541	1.674
	0.2	0.590	0.534	0.588	0.675	0.783	0.919	1.088	1.402	1.602
	0.3	0.473	0.430	0.473	0.548	0.648	0.776	0.945	1.289	1.543
	0.4	0.391	0.358	0.392	0.459	0.553	0.675	0.845	1.206	1.504
	0.5	0.330	0.305	0.333	0.394	0.484	0.604	0.777	1.151	1.489
	0.6	0.285	0.266	0.289	0.346	0.434	0.553	0.730	1.116	1.493
	0.7	0.251	0.237	0.256	0.311	0.400	0.519	0.702	1.105	1.523
	0.8	0.228	0.217	0.233	0.288	0.378	0.501	0.701	1.147	1.621
	0.9	0.215	0.206	0.221	0.277	0.374	0.512	0.758	1.293	1.857
1.0	0.01	1.898	1.681	1.641	1.623	1.611	1.634	1.666	1.746	1.836
	0.1	1.576	1.400	1.383	1.393	1.418	1.478	1.551	1.690	1.805
	0.2	1.342	1.196	1.191	1.215	1.258	1.336	1.434	1.620	1.761
	0.3	1.179	1.053	1.053	1.082	1.133	1.219	1.331	1.552	1.714
	0.4	1.059	0.947	0.948	0.979	1.035	1.127	1.250	1.499	1.682
	0.5	0.966	0.864	0.866	0.899	0.961	1.060	1.192	1.464	1.669
	0.6	0.892	0.799	0.801	0.838	0.908	1.012	1.151	1.444	1.671
	0.7	0.833	0.747	0.751	0.793	0.869	0.979	1.127	1.444	1.694
	0.8	0.788	0.707	0.713	0.761	0.846	0.964	1.132	1.492	1.778
	0.9	0.757	0.680	0.689	0.745	0.844	0.985	1.201	1.633	1.970
2.0	0.01	1.310	1.189	1.138	1.084	1.023	0.973	0.923	0.896	0.953
	0.1	1.194	1.087	1.051	1.015	0.973	0.940	0.906	0.897	0.961
	0.2	1.087	0.997	0.972	0.949	0.920	0.899	0.878	0.886	0.955
	0.3	1.001	0.922	0.905	0.889	0.869	0.857	0.845	0.868	0.943
	0.4	0.931	0.860	0.847	0.836	0.824	0.820	0.817	0.853	0.933
	0.5	0.873	0.809	0.799	0.792	0.786	0.790	0.795	0.844	0.929
	0.6	0.825	0.766	0.758	0.757	0.757	0.767	0.779	0.838	0.930
	0.7	0.785	0.731	0.726	0.728	0.735	0.750	0.768	0.840	0.938
	0.8	0.753	0.702	0.700	0.707	0.720	0.742	0.769	0.861	0.970
	0.9	0.730	0.681	0.682	0.695	0.718	0.751	0.799	0.919	1.043

Table 18 Dimensionless stress intensity factors for double corner cracks at a hole under wedge loading, r/t=2.5

a/c	a/t	$\varphi°$ 0.1	11.3	22.5	33.8	45.0	56.3	67.5	82.5	89.9
0.2	0.01	0.864	0.860	1.056	1.226	1.370	1.501	1.610	1.731	1.782
	0.1	0.530	0.529	0.659	0.791	0.928	1.083	1.256	1.536	1.689
	0.2	0.378	0.379	0.474	0.579	0.698	0.841	1.022	1.373	1.613
	0.3	0.287	0.292	0.364	0.452	0.557	0.689	0.867	1.246	1.552
	0.4	0.227	0.232	0.289	0.365	0.460	0.584	0.761	1.156	1.517
	0.5	0.184	0.191	0.236	0.303	0.391	0.511	0.689	1.098	1.507
	0.6	0.154	0.162	0.199	0.259	0.343	0.460	0.641	1.064	1.520
	0.7	0.132	0.142	0.172	0.228	0.310	0.426	0.612	1.058	1.564
	0.8	0.118	0.130	0.155	0.208	0.290	0.408	0.611	1.112	1.688
	0.9	0.109	0.123	0.144	0.199	0.286	0.417	0.668	1.288	1.983
0.4	0.01	1.259	1.129	1.221	1.334	1.441	1.550	1.643	1.755	1.809
	0.1	0.951	0.854	0.935	1.045	1.164	1.302	1.444	1.647	1.749
	0.2	0.760	0.685	0.753	0.853	0.970	1.112	1.275	1.541	1.690
	0.3	0.638	0.576	0.635	0.724	0.835	0.975	1.145	1.451	1.640
	0.4	0.551	0.499	0.549	0.631	0.737	0.874	1.050	1.387	1.612
	0.5	0.483	0.440	0.483	0.560	0.665	0.804	0.987	1.349	1.610
	0.6	0.431	0.393	0.432	0.507	0.614	0.756	0.946	1.332	1.628
	0.7	0.389	0.357	0.393	0.467	0.578	0.724	0.927	1.342	1.677
	0.8	0.357	0.330	0.363	0.440	0.556	0.713	0.942	1.418	1.809
	0.9	0.336	0.313	0.344	0.426	0.555	0.738	1.034	1.631	2.109
1.0	0.01	1.968	1.742	1.699	1.679	1.664	1.685	1.716	1.794	1.885
	0.1	1.755	1.553	1.526	1.526	1.536	1.583	1.641	1.757	1.863
	0.2	1.569	1.392	1.377	1.390	1.416	1.480	1.557	1.707	1.829
	0.3	1.424	1.266	1.257	1.276	1.313	1.386	1.480	1.658	1.795
	0.4	1.308	1.165	1.159	1.182	1.227	1.310	1.418	1.624	1.776
	0.5	1.215	1.083	1.079	1.107	1.161	1.255	1.376	1.608	1.776
	0.6	1.140	1.017	1.016	1.049	1.113	1.218	1.351	1.608	1.793
	0.7	1.079	0.964	0.966	1.007	1.081	1.196	1.342	1.629	1.835
	0.8	1.033	0.924	0.930	0.979	1.066	1.194	1.367	1.711	1.948
	0.9	1.003	0.899	0.909	0.969	1.076	1.236	1.470	1.909	2.197
2.0	0.01	1.351	1.225	1.172	1.116	1.052	0.999	0.947	0.919	0.977
	0.1	1.278	1.161	1.116	1.071	1.020	0.979	0.937	0.919	0.982
	0.2	1.204	1.097	1.061	1.026	0.984	0.951	0.918	0.911	0.977
	0.3	1.138	1.040	1.011	0.982	0.947	0.921	0.896	0.900	0.969
	0.4	1.081	0.990	0.965	0.941	0.913	0.895	0.877	0.892	0.965
	0.5	1.031	0.946	0.925	0.906	0.885	0.875	0.866	0.891	0.967
	0.6	0.988	0.909	0.891	0.877	0.864	0.862	0.859	0.894	0.975
	0.7	0.951	0.878	0.863	0.856	0.850	0.854	0.858	0.904	0.991
	0.8	0.922	0.853	0.842	0.841	0.843	0.856	0.871	0.939	1.036
	0.9	0.901	0.835	0.829	0.835	0.850	0.879	0.919	1.017	1.130

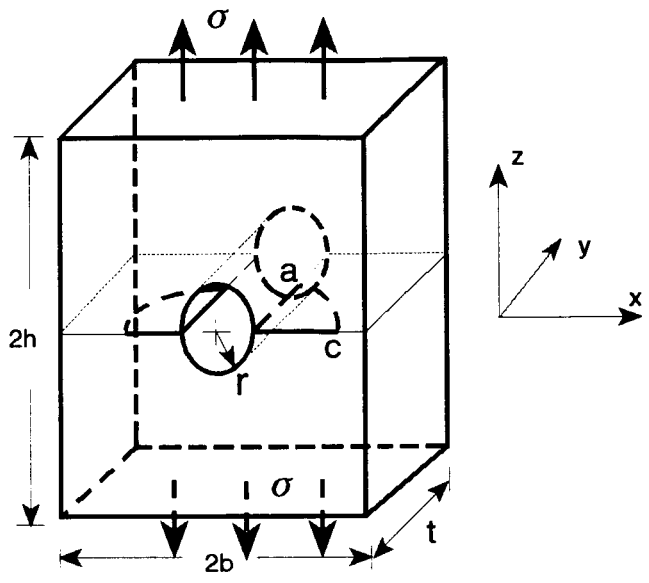

Fig.1 Double corner cracks at a hole under remote tension

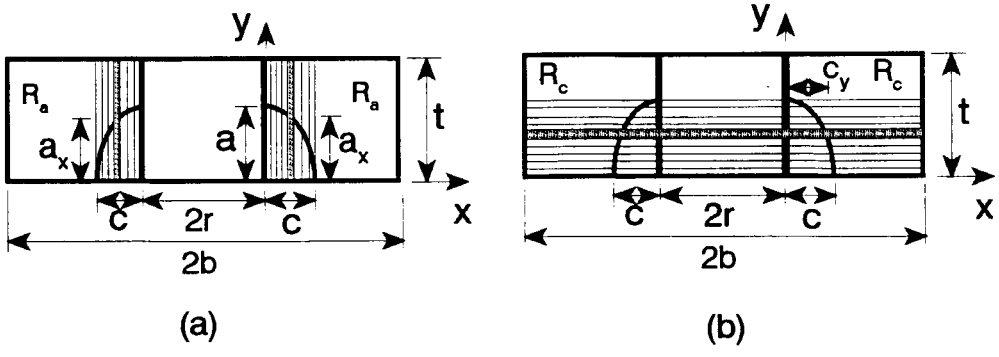

Fig. 2 Decomposition of the corner cracked body into
(a) a-slice, (b) c-slice

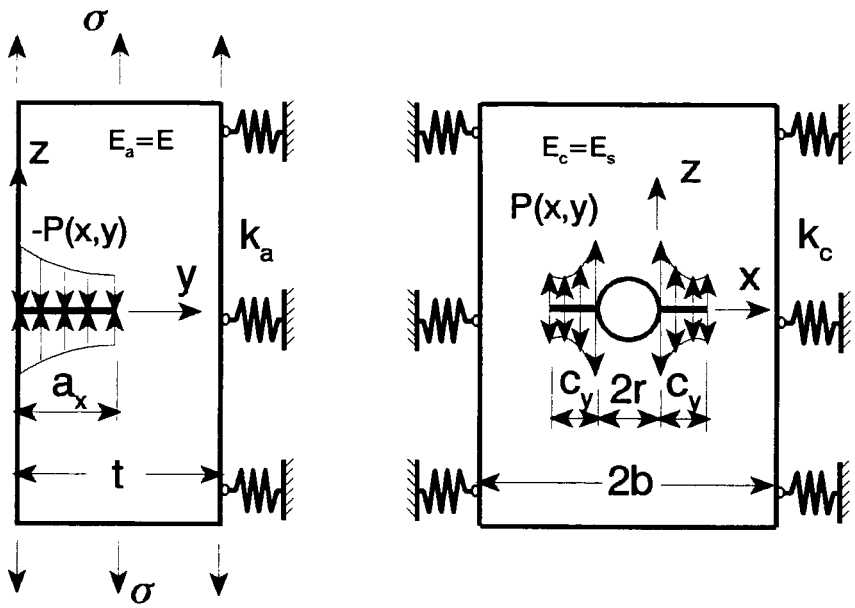

(a) (b)

Fig.3 $0<k_i<\infty$, (a) a-slice, (b) c-slice.

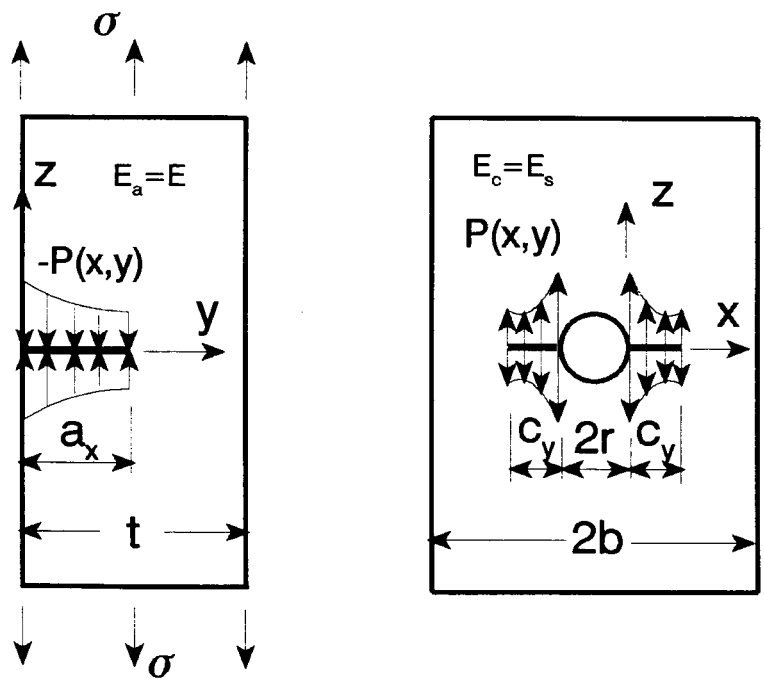

(a) (b)

Fig.4 $k_i=0$, (a) a-slice, (b) c-slice.

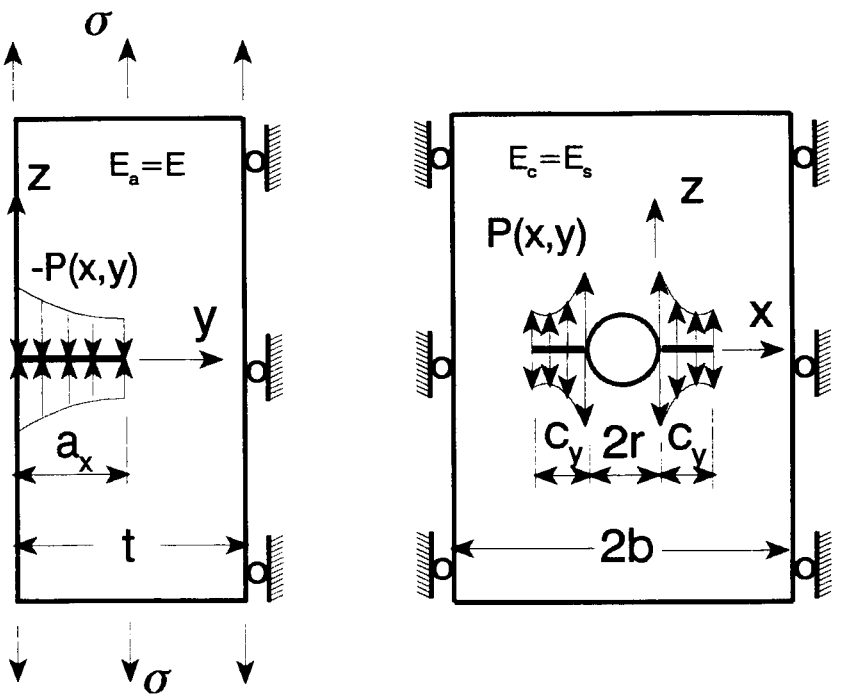

(a) (b)

Fig.5 $k_i=\infty$, (a) a-slice, (b) c-slice.

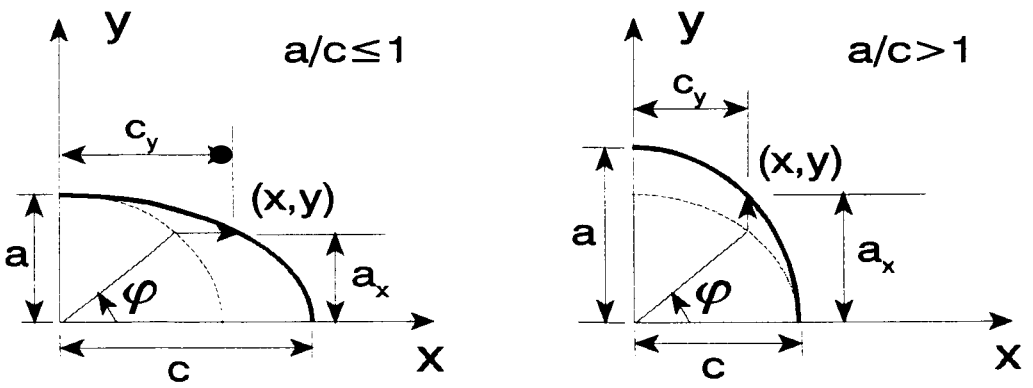

Fig.6 Definition of crack parameters

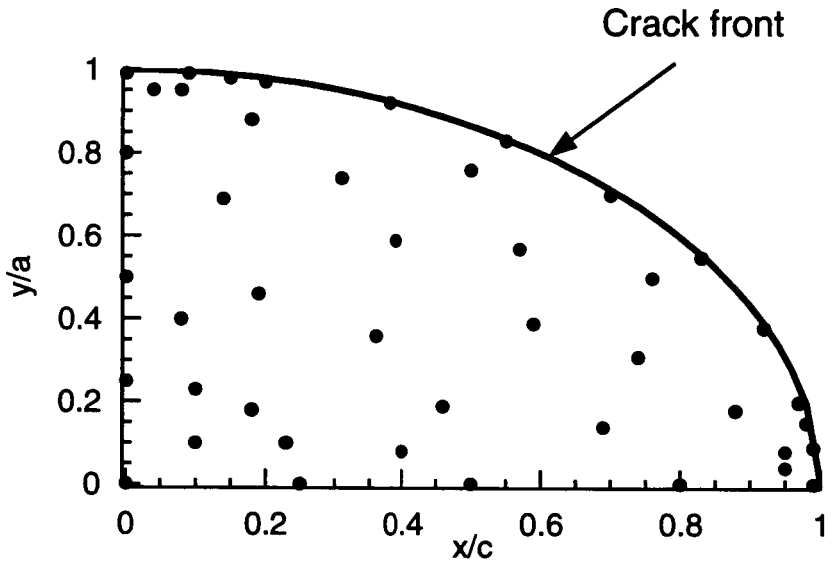

Fig. 7 Points on the crack surface where displacements are evaluated.

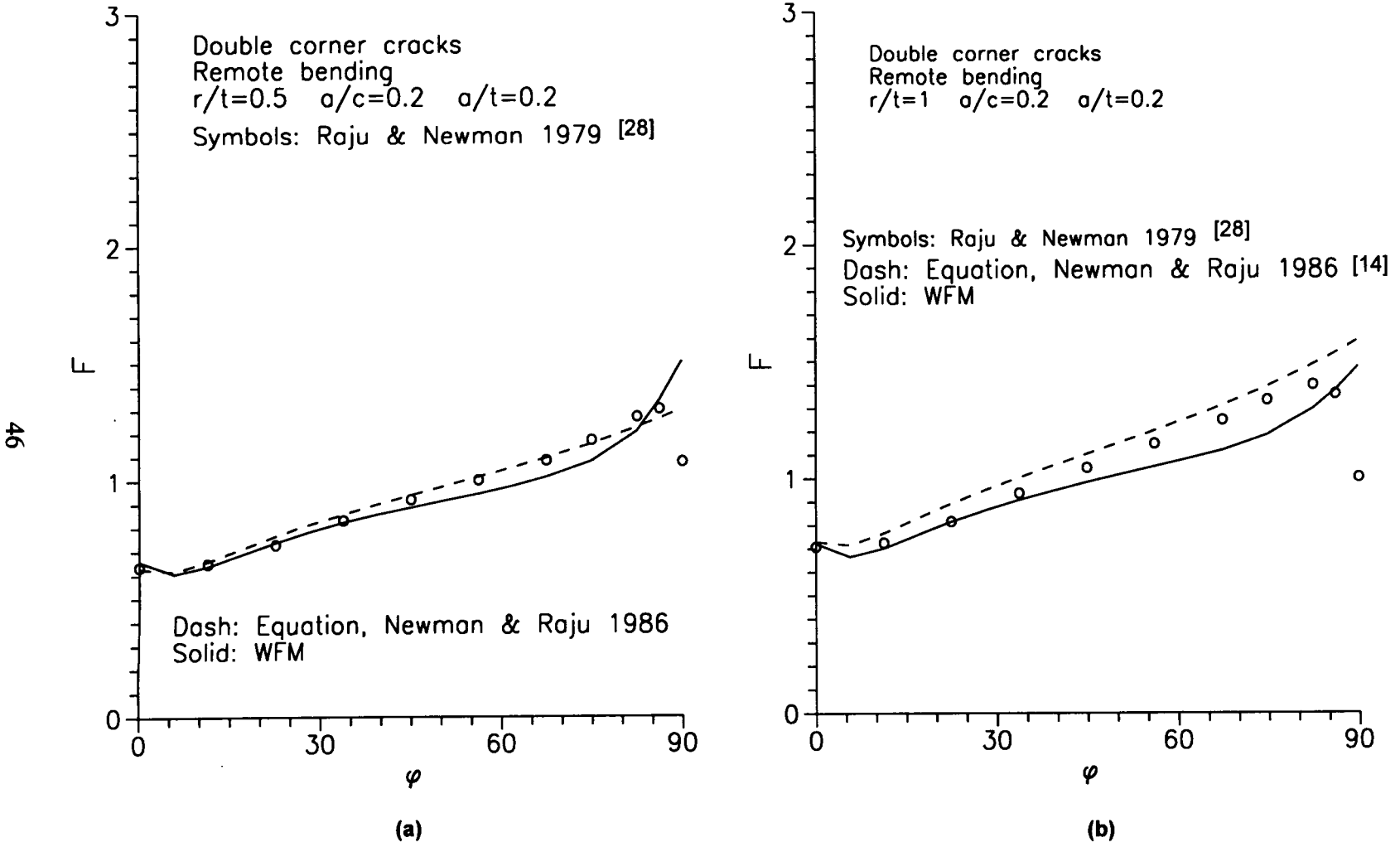

Fig.8 Dimensionless stress intensity factors for double corner cracks under remote bending, a/c=0.2

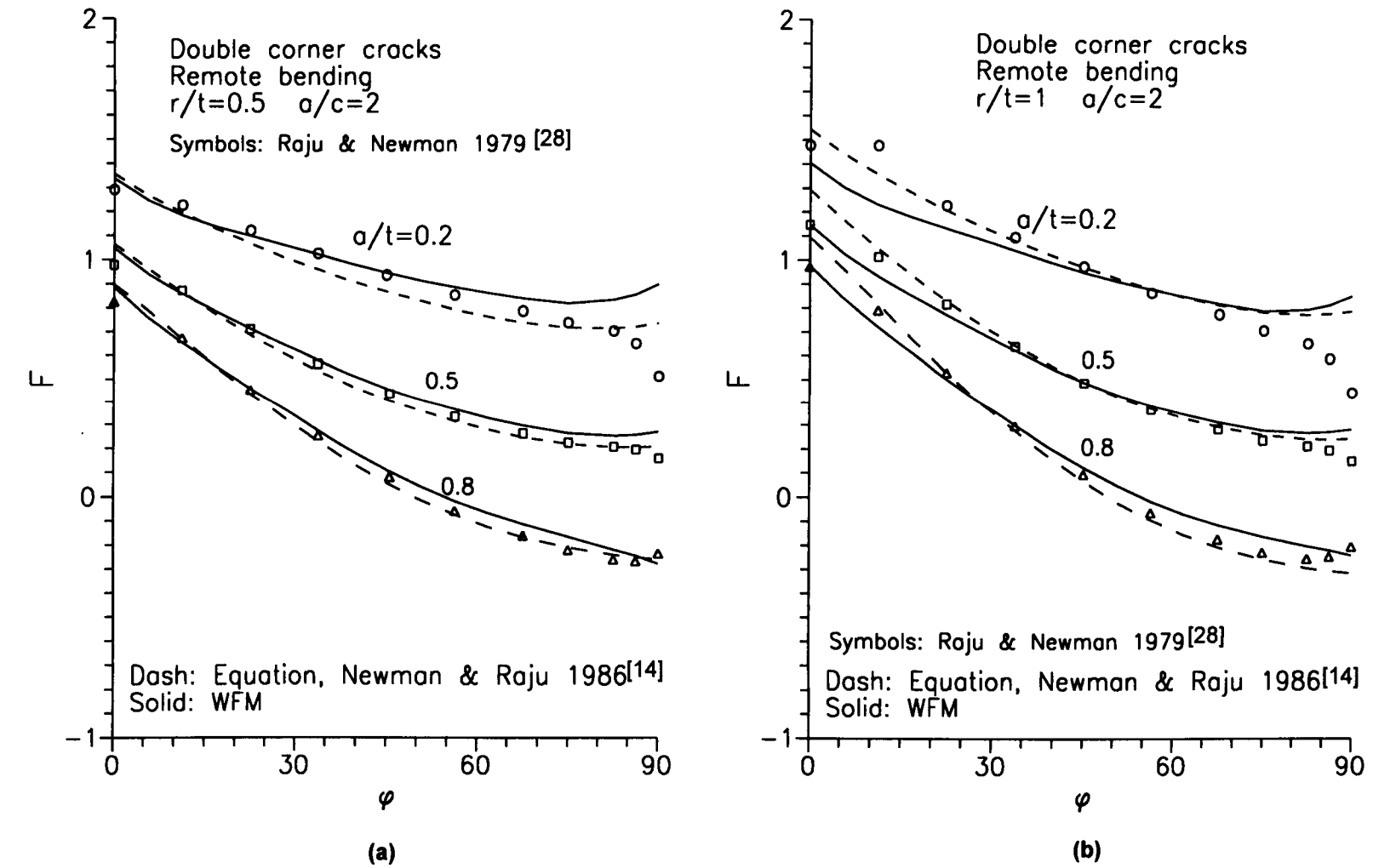

Fig. 9 Stress intensity factors for double corner cracks under remote bending, a/c=2

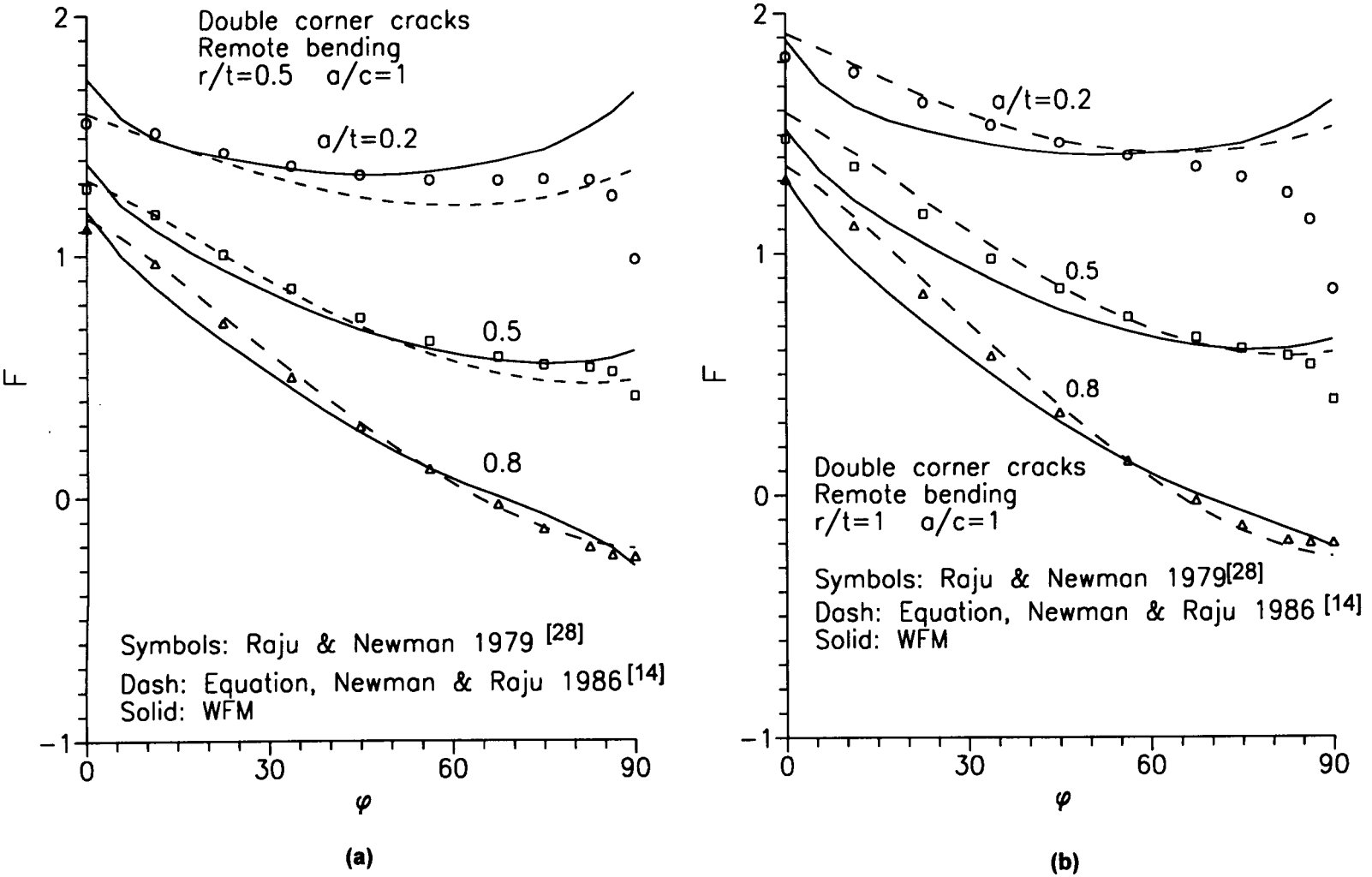

Fig.10 Stress intensity factors for double corner cracks under remote bending, a/c=1

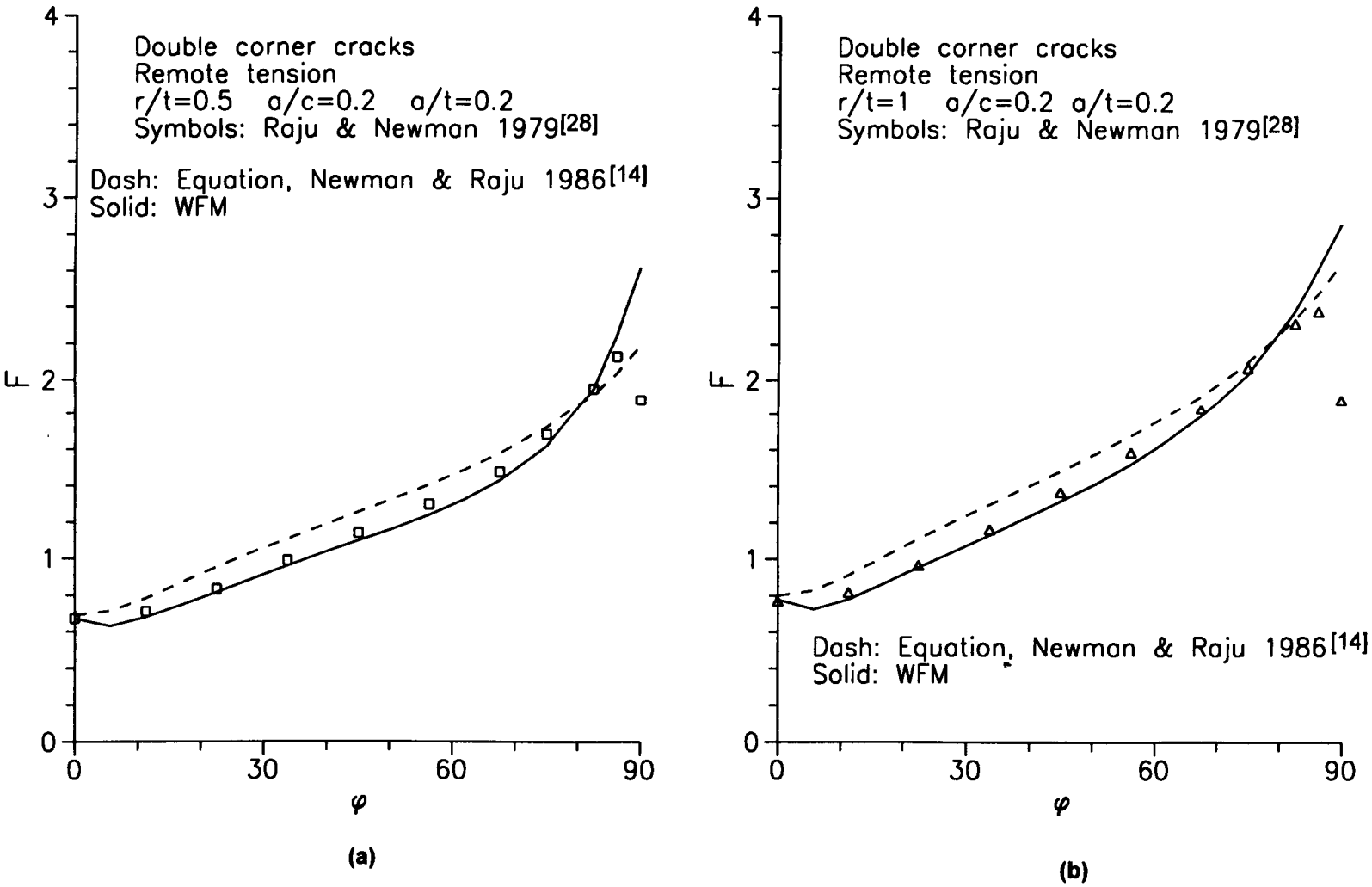

Fig.11 Stress intensity factors for double corner cracks under remote tension, a/c=0.2

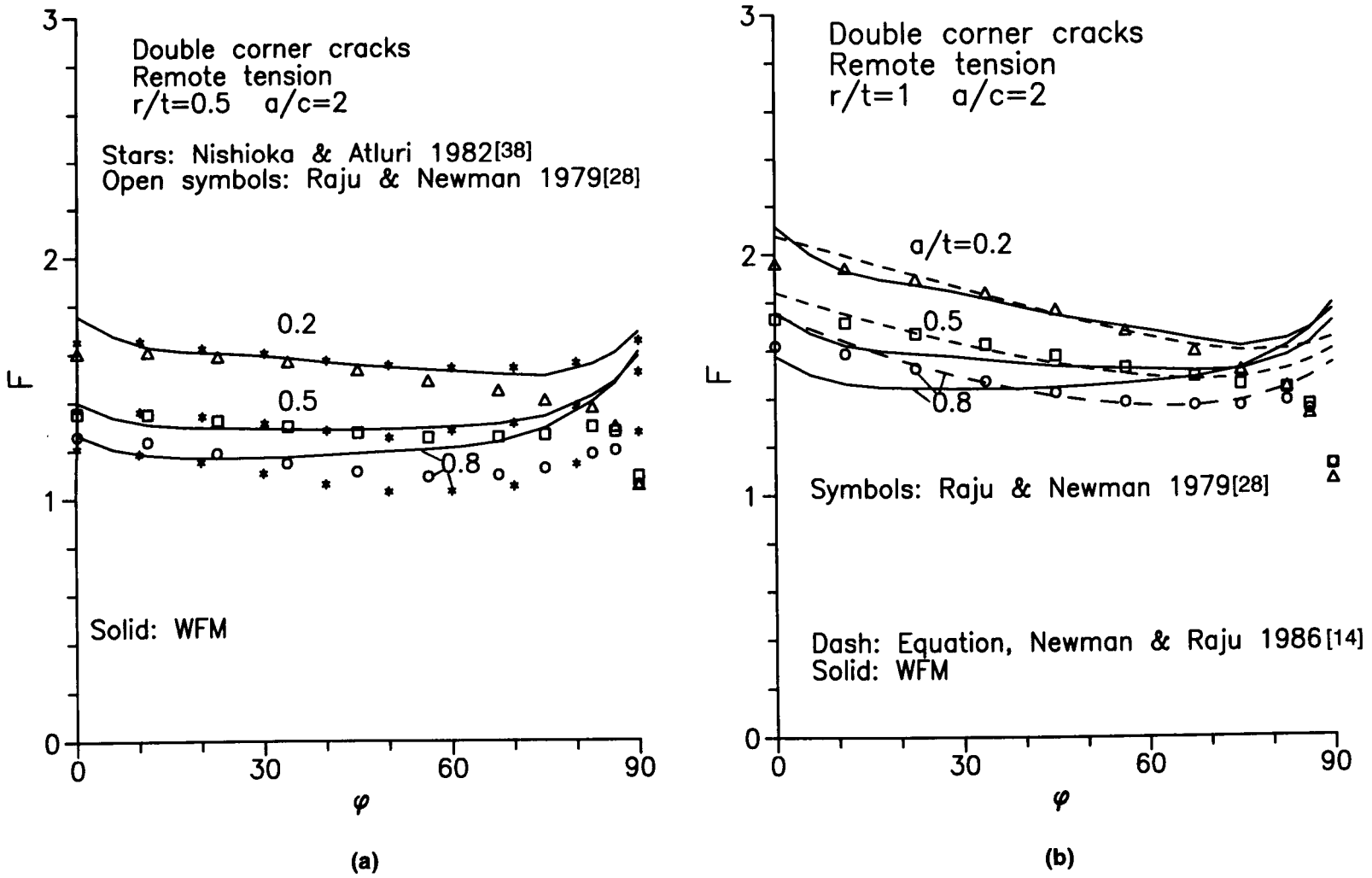

Fig.12 Stress intensity factors for double corner cracks under remote tension, a/c=2

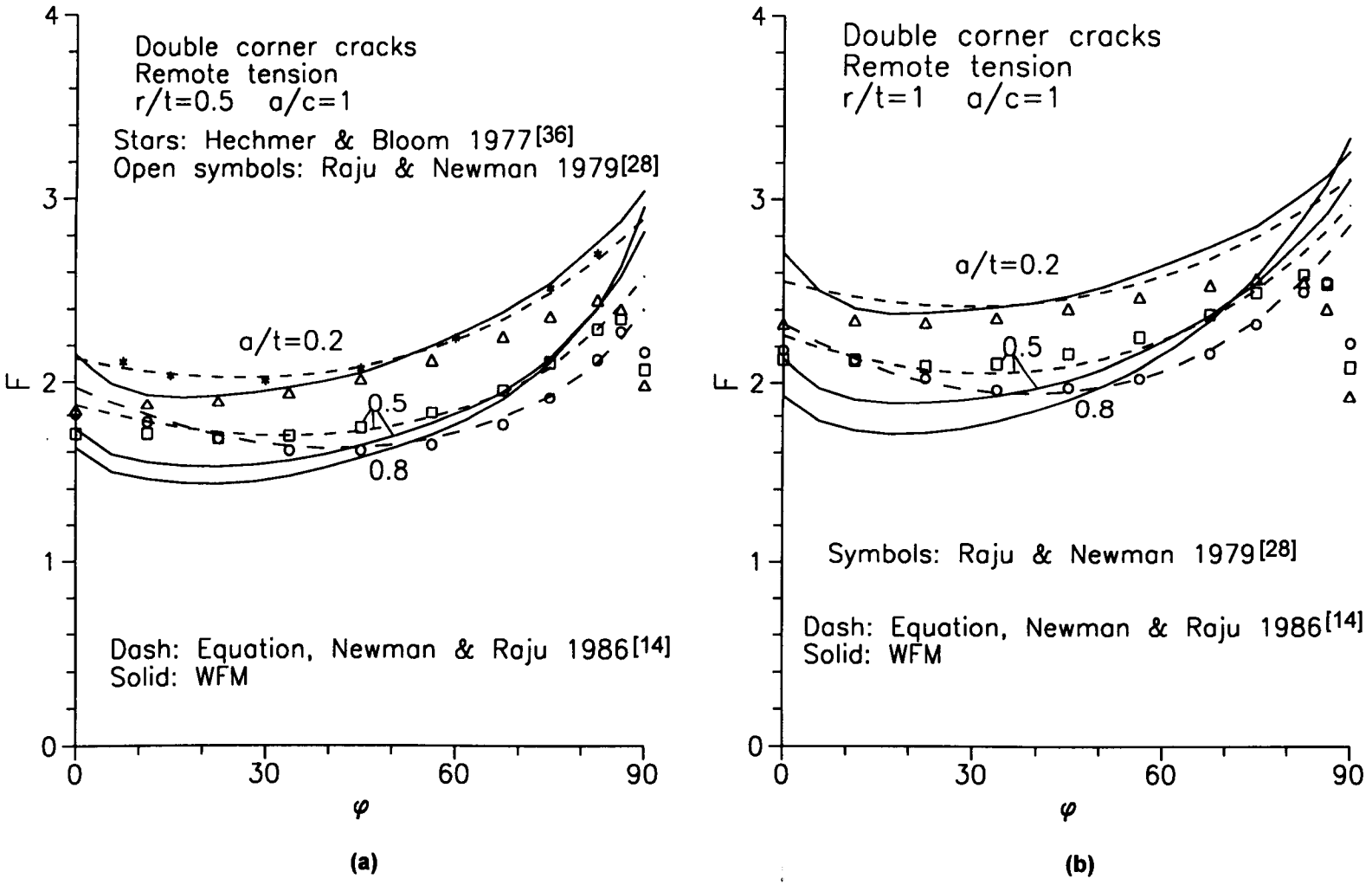

Fig.13 Stress intensity factors for double corner cracks under remote tension, a/c=1

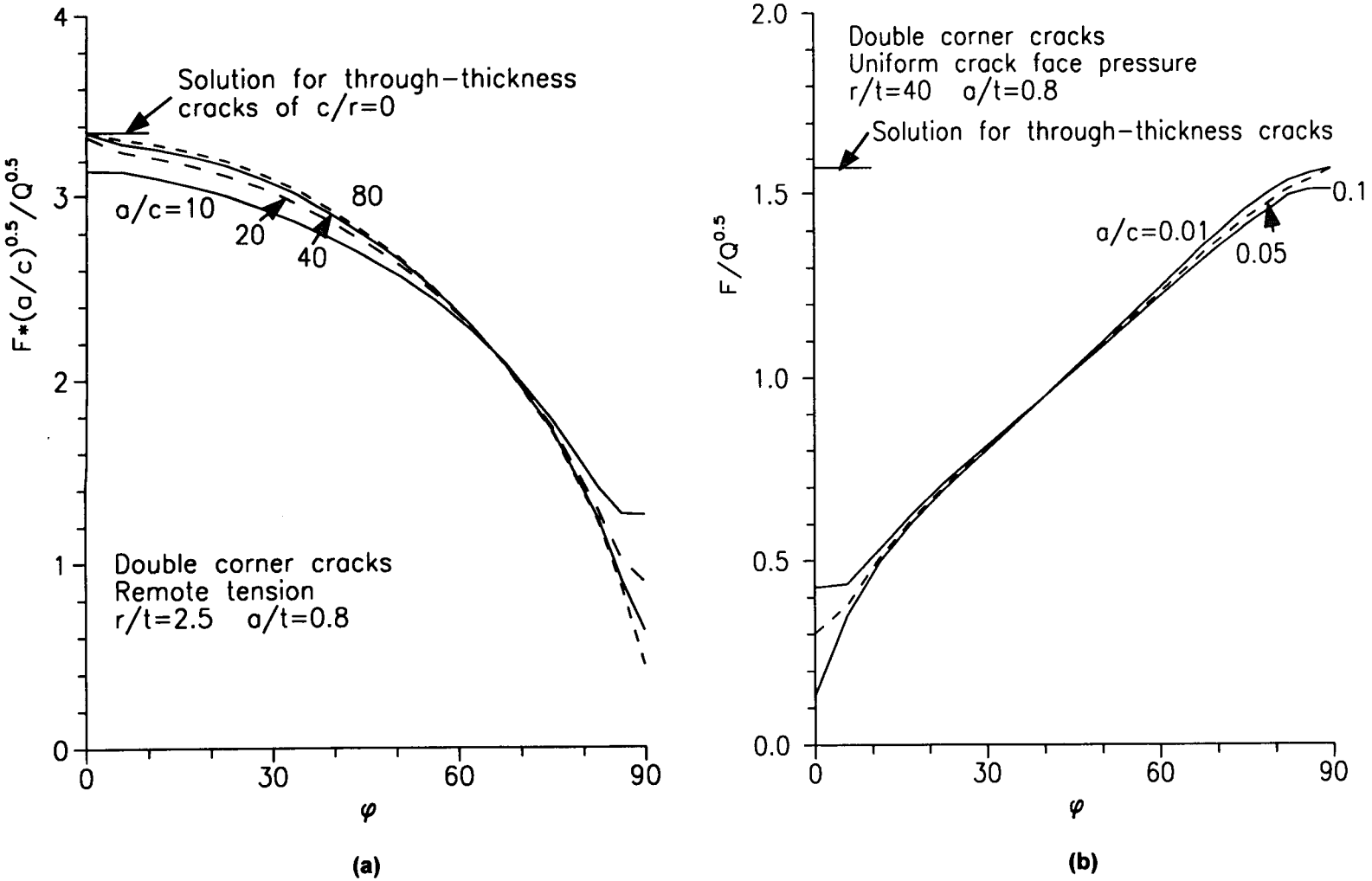

Fig.14 Limiting behavior of corner cracks under remote tension

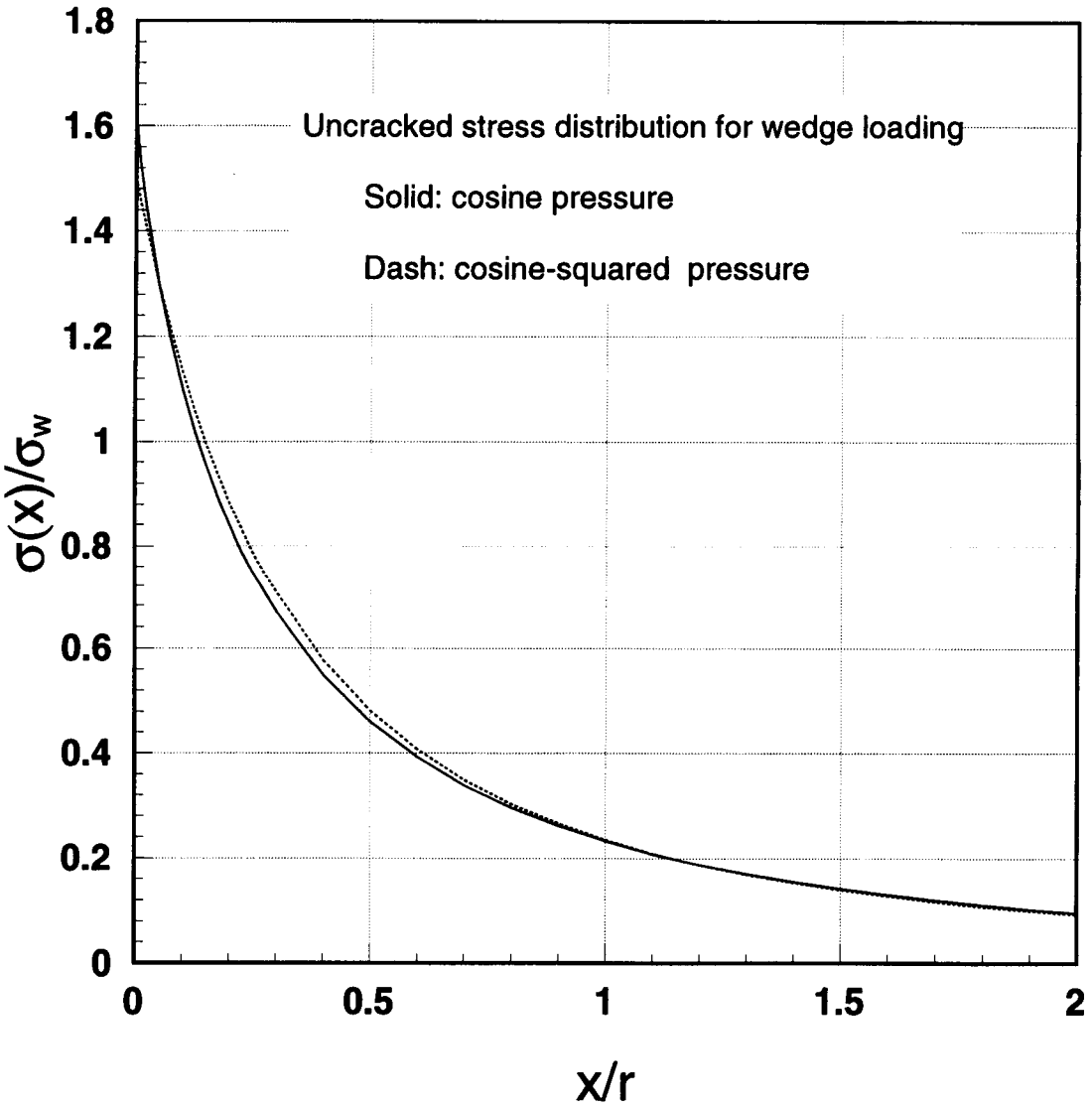

Fig. 15 Comparison of uncracked stress distributions for different wedge loadings in the hole (2-D solution).

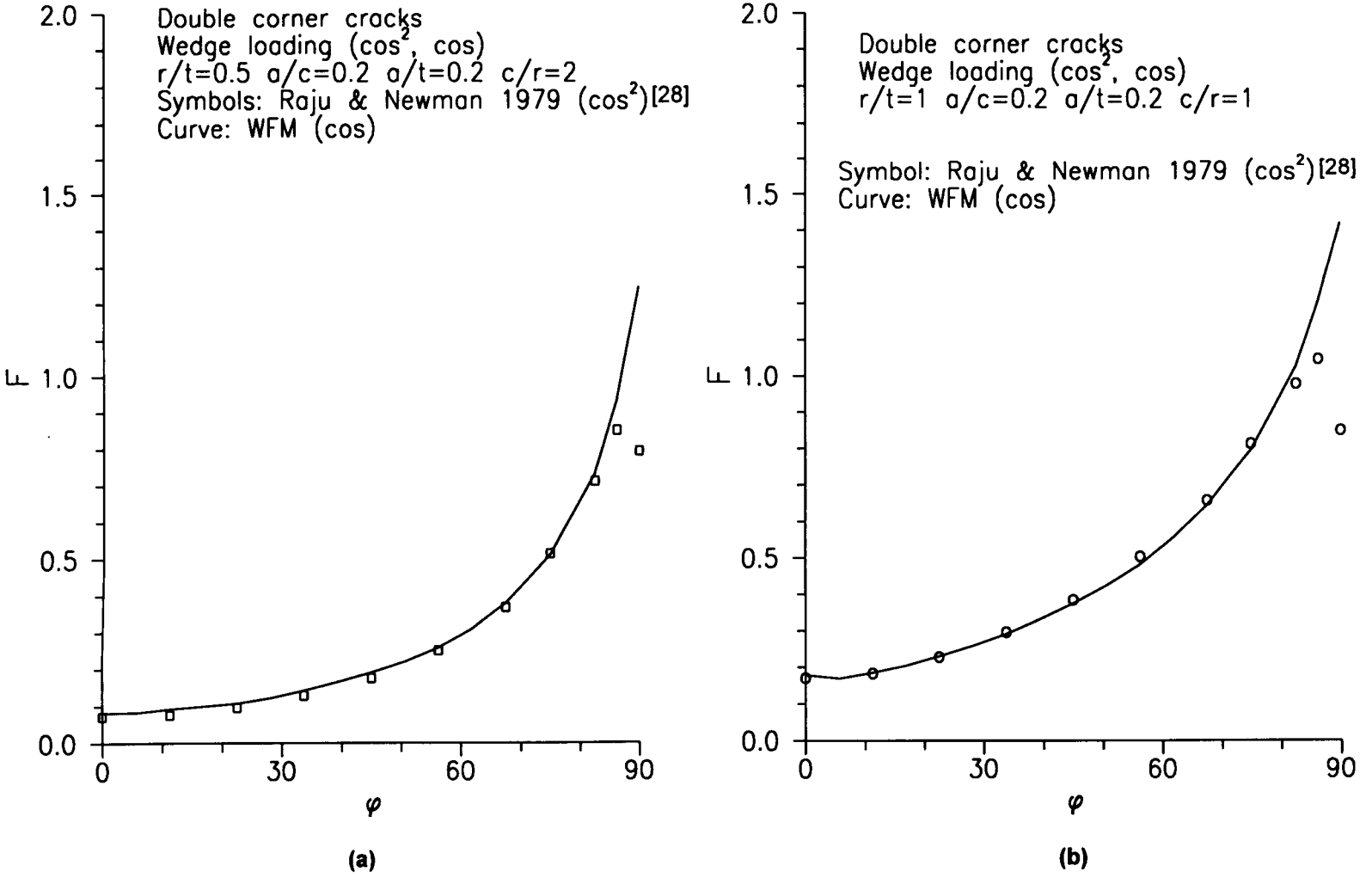

Fig.16 Stress intensity factors for double corner cracks under wedge loading, a/c=0.2

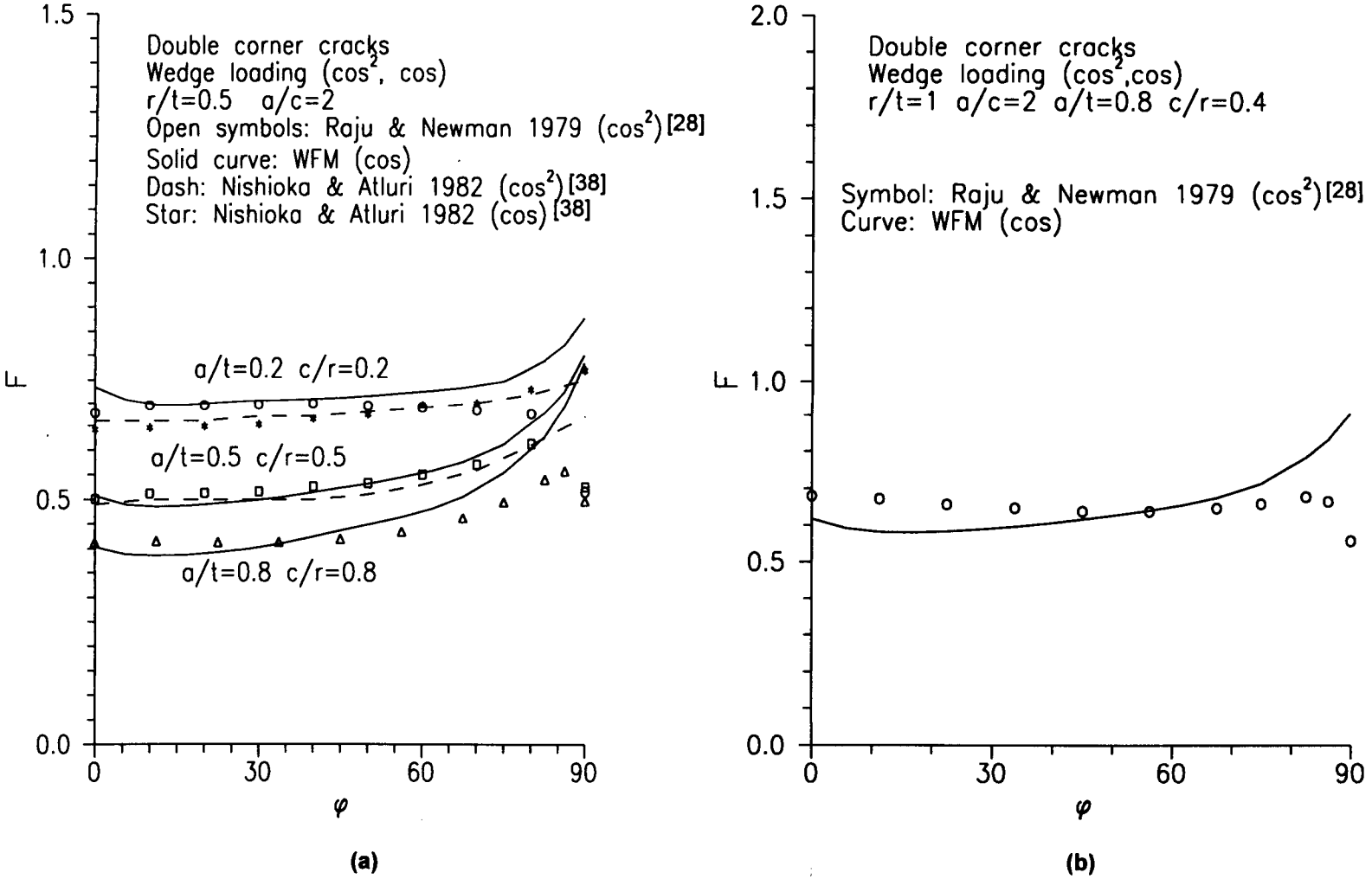

Fig.17 Stress intensity factors for double corner cracks under wedge loading, a/c=2

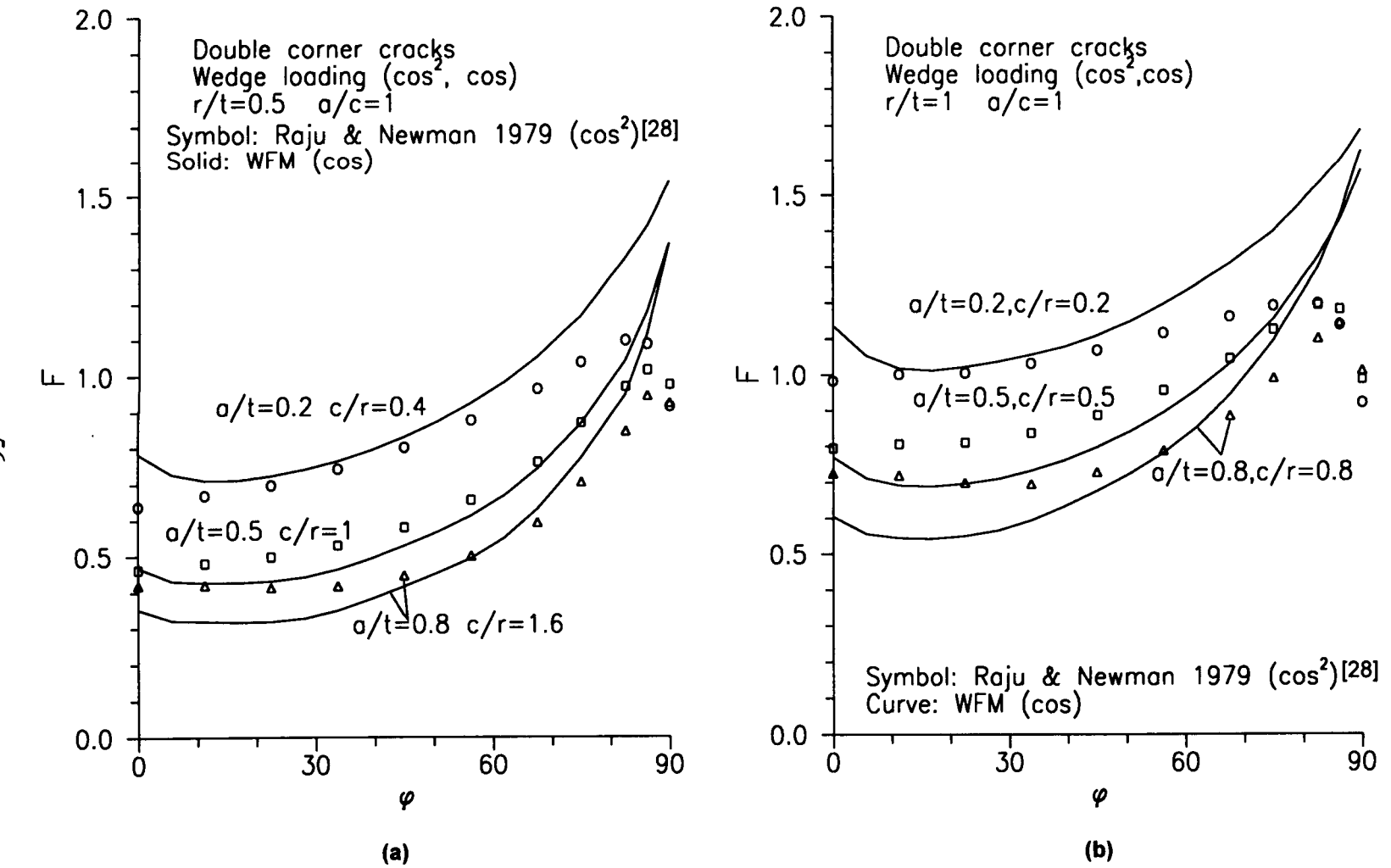

Fig.18 Stress intensity factors for double corner cracks under wedge loading, a/c=1

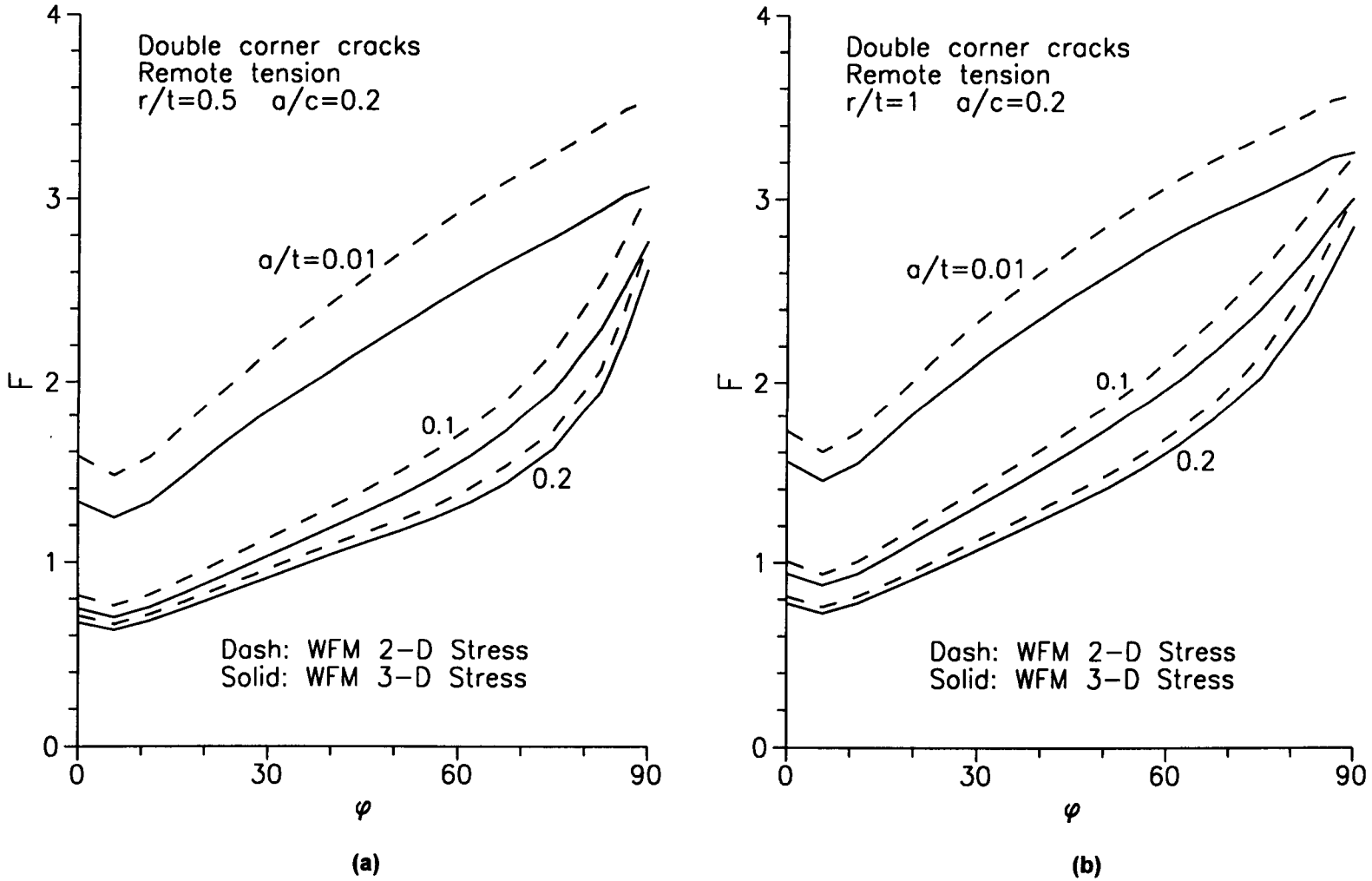

Fig.19 Comparison of solutions obtained by using 2-D and 3-D stress distributions, (a) r/t=0.5, (b) r/t=1

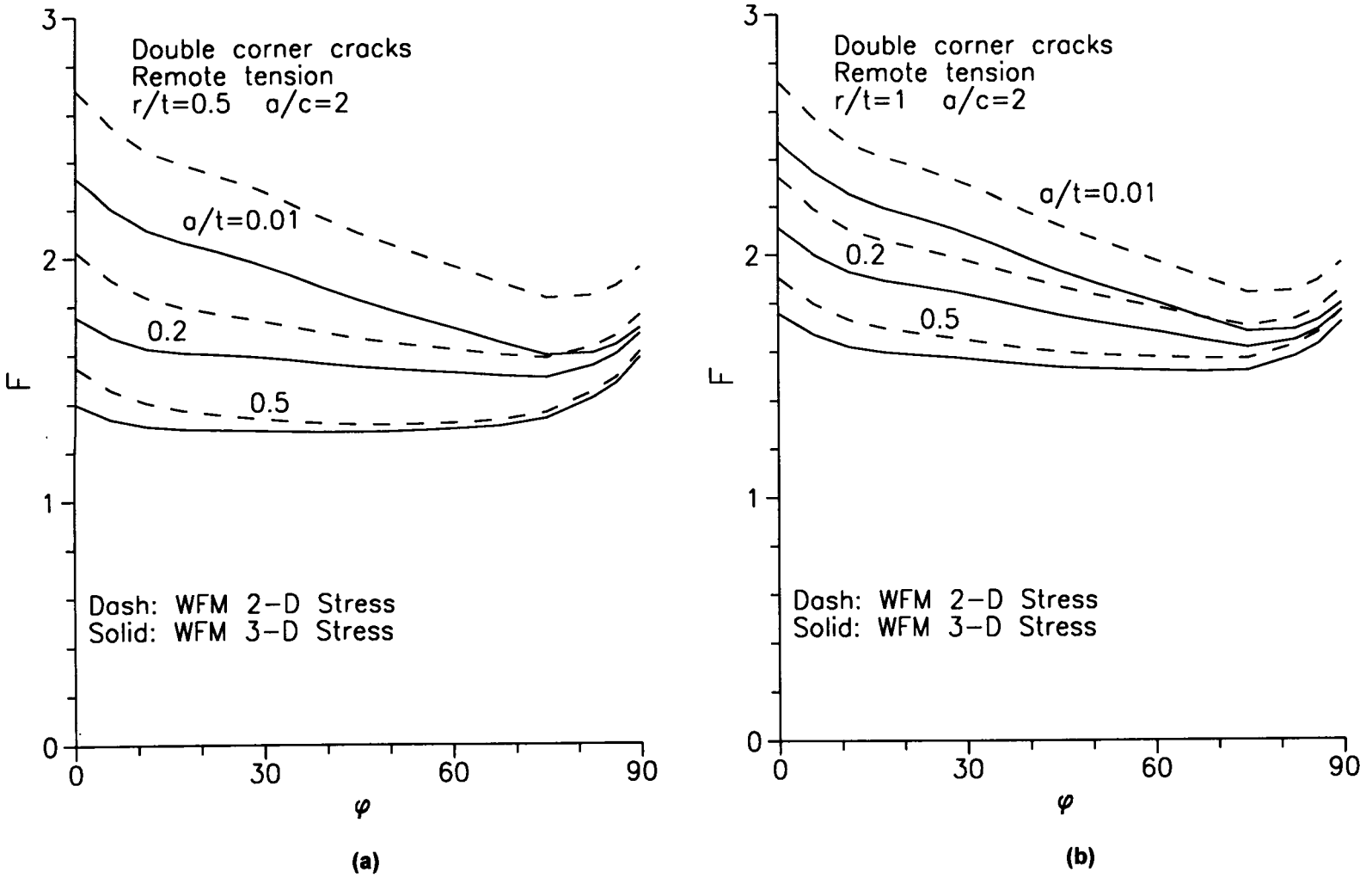

Fig.20 Comparison of solutions obtained by using 2-D and 3-D stress distributions, (a) r/t=0.5, (b) r/t=1

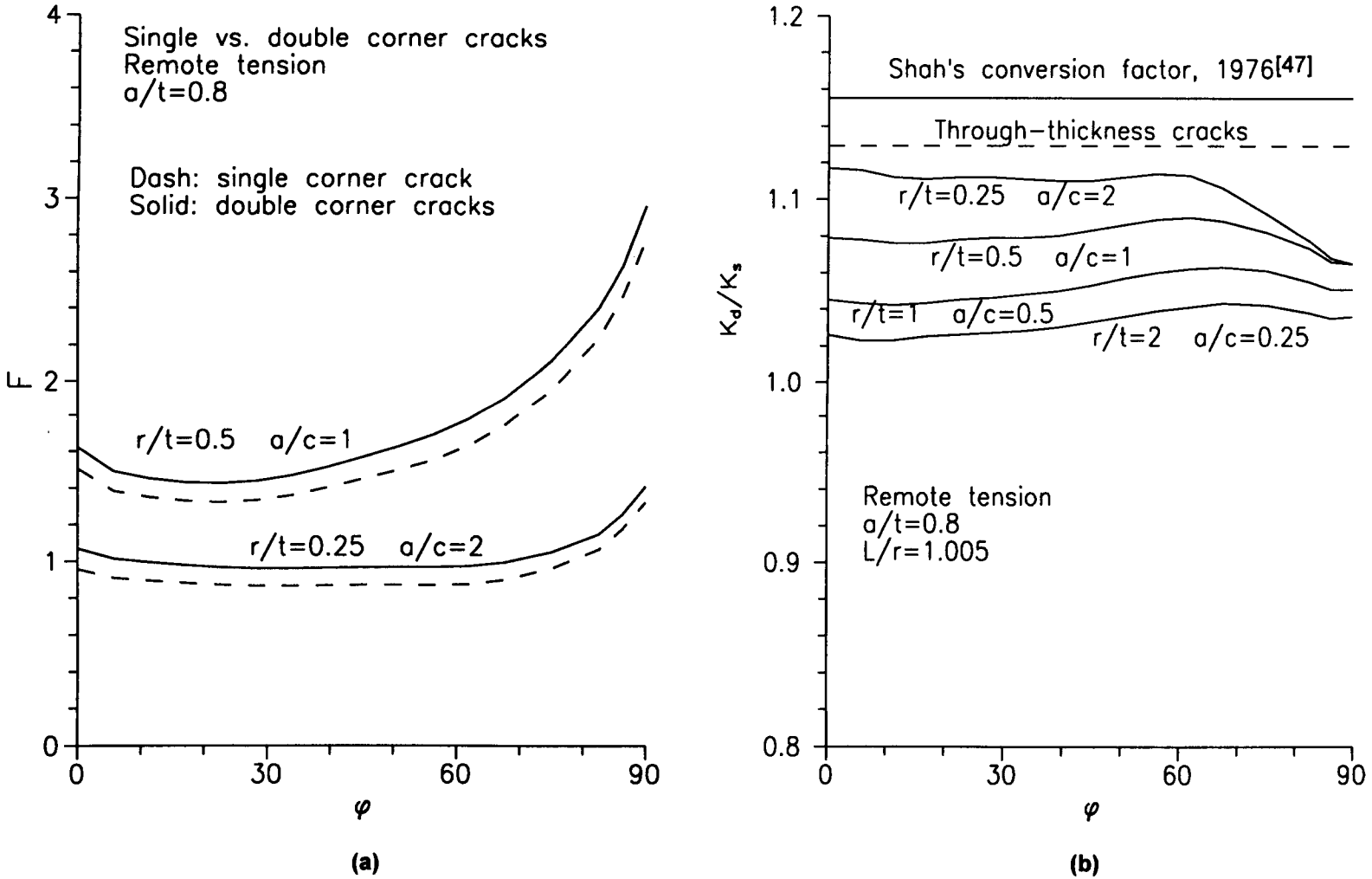

Fig.21 Comparison between single and double corner cracks under remote tension, (a) F factor (b) ratio

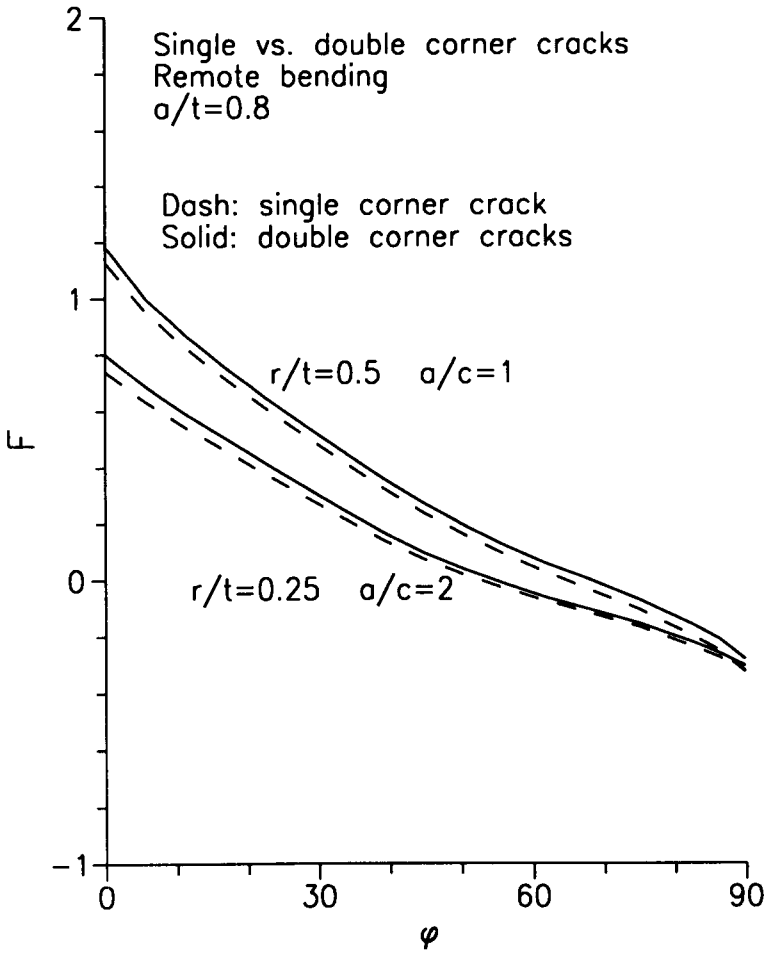

Fig.22 Comparison between single and double corner cracks under remote bending

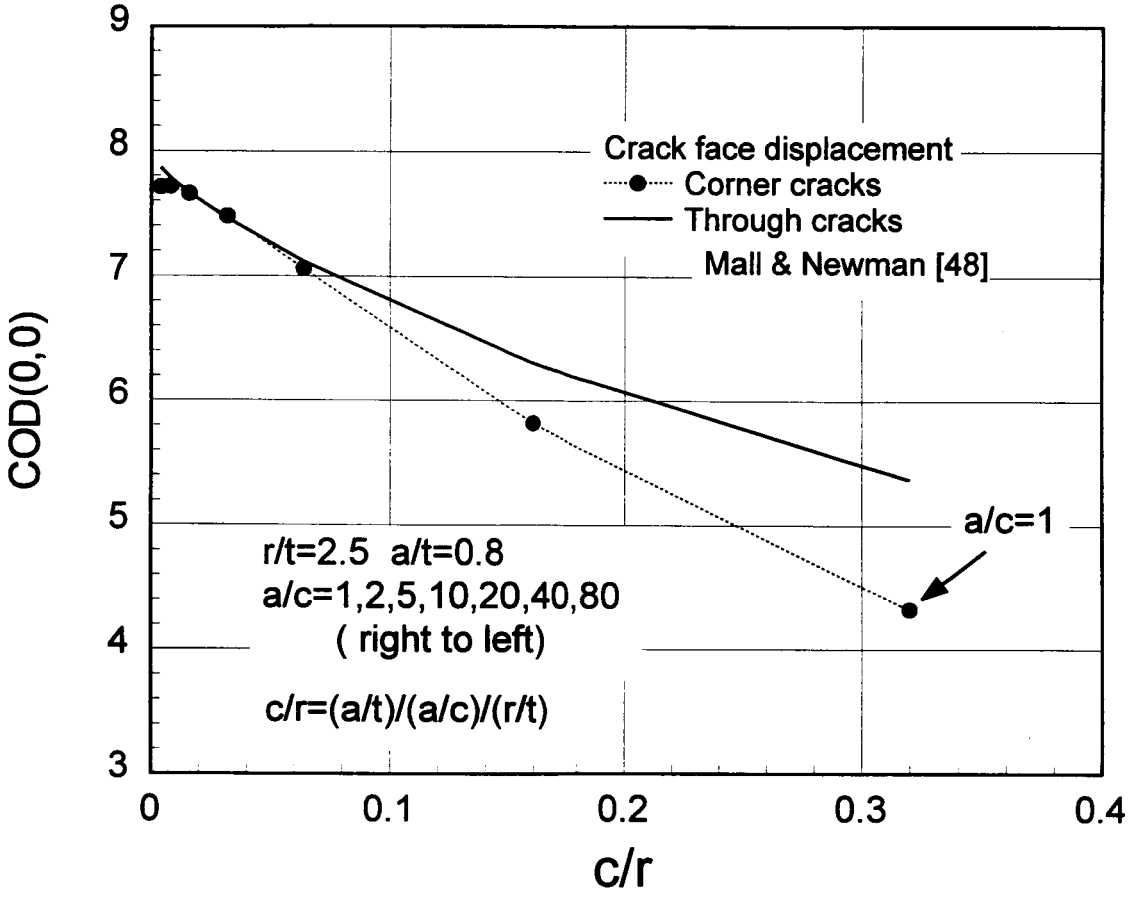

Fig.23 Normalized crack mouth displacement under remote tension

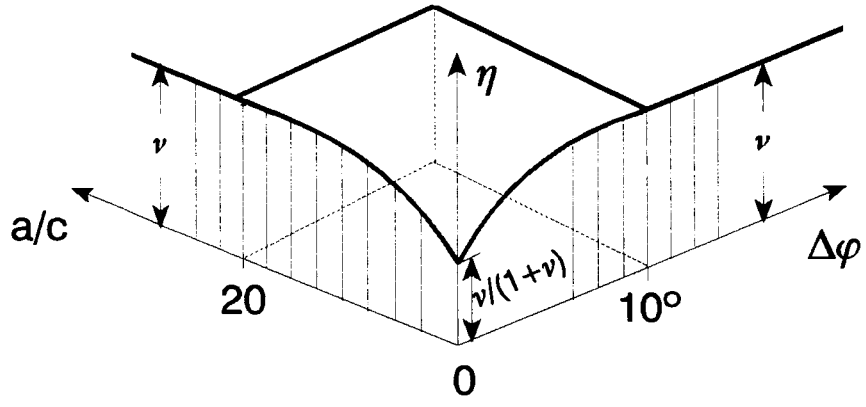

Fig.B1. Schematic representation of the interpolation function.

REPORT DOCUMENTATION PAGE

Form Approved
OMB No. 0704-0188

1. AGENCY USE ONLY (*Leave blank*)	2. REPORT DATE	3. REPORT TYPE AND DATES COVERED
	July 1995	Technical Memorandum

4. TITLE AND SUBTITLE
Analysis of Corner Cracks at Hole by a 3-D Weight Function Method with Stresses from Finite Element Method

5. FUNDING NUMBERS
WU 538-02-10-01

6. AUTHOR(S)
W. Zhao, J. C. Newman, Jr., M. A. Sutton, X. R. Wu, and K. N. Shivakumar

7. PERFORMING ORGANIZATION NAME(S) AND ADDRESS(ES)
NASA Langley Research Center
Hampton, VA 23681-0001

8. PERFORMING ORGANIZATION REPORT NUMBER

9. SPONSORING / MONITORING AGENCY NAME(S) AND ADDRESS(ES)
National Aeronautics and Administration
Washington, DC 20546-0001

10. SPONSORING / MONITORING AGENCY REPORT NUMBER
NASA TM-110144

11. SUPPLEMENTARY NOTES
Zhao: University of South Carolina, Columbia, SC; Newman: Langley Research Center, Hampton, VA; Sutton: University of South Carolina, Columbia, SC; Wu: Institute of Aeronautical Materials, Beijing, Peoples of China; Shivakumar: North Carolina A&T State University, Greensboro, NC.

12a. DISTRIBUTION / AVAILABILITY STATEMENT
Unclassified - Unlimited

Subject Category 24

12b. DISTRIBUTION CODE

13. ABSTRACT (*Maximum 200 words*)

Stress intensity factors for quarter-elliptical corner cracks emanating from a circular hole are determined using a 3-D weight function method combined with a 3-D finite element method. The 3-D finite element method is used to analyze uncracked configuration and provide stress distribution in the region where crack is to occur. Using this stress distribution as input, the 3-D weight function method is used to determine stress intensity factors. Three different loading conditions, i.e. remote tension, remote bending and wedge loading, are considered for a wide range in geometrical parameters. The significance in using 3-D uncracked stress distribution and the difference between single and double corner cracks are studied. Typical crack opening displacements are also provided. Comparisons are made with solutions available in the literature.

14. SUBJECT TERMS
Stress-intensity factor; Weight functions; Finite-element method; Corner crack

15. NUMBER OF PAGES
63

16. PRICE CODE
A04

17. SECURITY CLASSIFICATION OF REPORT	18. SECURITY CLASSIFICATION OF THIS PAGE	19. SECURITY CLASSIFICATION OF ABSTRACT	20. LIMITATION OF ABSTRACT
Unclassified	Unclassified		